NVE

EKSTERN RAPPORT NR. 12 / 2024

Stability evaluation of toe supported ripraps exposed to overtopping

Report R&D-project 80418, part 1

BY Théo Dezert and Fjóla G. Sigtryggsdóttir

NVE Ekstern rapport nr. 12/2024
Stability evaluation of toe supported ripraps exposed to overtopping : report R&D-project 80418, part 1

Utgitt av:	Norges vassdrags- og energidirektorat
Forfattere:	Théo Dezert and Fjóla G. Sigtryggsdóttir, NTNU
Omslagsfoto:	Oppgradering av dam Gråsjø. Foto: Grethe Holm Midttømme/NVE
ISBN:	978-82-410-2388-0
ISSN:	2535-8235
Saksnummer:	202110167

Sammendrag:	Rapporten summerer opp og supplerer tidligere forskning utført ved vassdragslaboratoriet på NTNU, Trondheim. Den viser hvordan nedstrøms plastring og damtå på fyllingsdammer innvirker på sikkerhet mot brudd som skyldes overtopping av damkrone.

Emneord:	Damsikkerhet, fyllingsdam, plastring, damtå, stabilitet, fysiske modellforsøk

Norges vassdrags- og energidirektorat
Middelthuns gate 29
Postboks 5091 Majorstuen
0301 Oslo

Telefon: 22 95 95 95
E-post: nve@nve.no
Internett: www.nve.no

April 2024

Forord

Siden 2013 har det vært utført omfattende forskning på fyllingsdammer ved NTNU, vassdragslaboratoriet i Trondheim. Det har resultert i flere doktoravhandlinger og Masteroppgaver, samt en rekke vitenskapelige artikler. Et hovedmål med FoU-prosjekt «Nedstrøms plastring, damtå og bruddforløp» har vært å få økt kunnskap om laster på nedstrøms plastring og damtå på steinfyllingsdammer, og om bruddforløp på steinfyllingsdammer med og uten plastring. I del 1 av prosjektet, som er presentert i denne rapporten, har det vært fokus på nedstrøms plastring og damtå. Prosjektet (del 1) har sammenstilt forskning som ble utført i perioden 2013-2022, og de resultatene som har kommet ut av laboratorieforsøkene og publikasjonene er supplert med nye laboratorieforsøk.

Arbeidene startet i 2022 som et post.doc-prosjekt utført av Théo Dezert. Prosjektleder har vært professor Fjóla Guðrún Sigtryggsdóttir. Den første delen av prosjektet har omfattet sammenstilling av resultater fra doktorgradsprosjektene til Priska Hiller og Ganesh Ravindra, samt resultater fra nye laboratorieforsøk utført i 2022 av post.doc. Théo Dezert. NVEs prosjektleder har vært Grethe Holm Midttømme.

NVE håper resultatene vil bidra til videreutvikling av veiledere og regelverk for fyllingsdammer.

Oslo, april 2024

Lars Grøttå
seksjonssjef
Seksjon for damsikkerhet
Tilsyns- og beredskapsavdelingen

Dokumentet sendes uten underskrift. Det er godkjent i henhold til interne rutiner.

Sammendrag

Fyllingsdammer er sårbare for hendelser som kan føre til økt gjennomstrømning og overtopping. Det kan medføre erosjon av fyllingsmassene og i verste fall dambrudd. Det norske regelverket stiller krav om sikring av fyllingsdammer mot erosjon og andre laster både på vannsiden (oppstrøms), over toppen av dammen (damkrona) og på luftsiden (nedstrøms). Videre er det krav om at skråningsvern av stein skal bygges som plastring, som innebærer at steinene skal være lagt i forband slik at steinene låser hverandre fast. Det er også krav om å vurdere behov for å sikre laveste del av skråningen (damtåa) og overgangen til vederlag med større stein eller andre tiltak.

Målet for dette prosjektet har vært å få økt kunnskap om laster på nedstrøms plastring og damtå, og om bruddforløp på steinfyllingsdammer med og uten plastring. Denne rapporten oppsummerer del 1 av prosjektet som omhandler laster på nedstrøms plastring og damtå.

Den viktigste funksjonen til nedstrøms skråningsvern er å hindre at underliggende fylling, støttefyllingen, blir erodert vekk av utstrømmende vann. Nedstrøms damtå blir mest utsatt og det er derfor viktig å kunne estimere lasten på tåstøtten. Problemstillingen har de siste årene vært undersøkt med modellforsøk utført ved vassdragslaboratoriet på NTNU, Trondheim. Rapporten viser til to tidligere PhD-prosjekter og tilknyttede masteroppgaver, og beskriver supplerende modellforsøk som er gjennomført nylig som del av et postdoktorprosjekt.

Modellforsøkene i postdoktorprosjektet er utført med to ulike modelloppsett, benevnt M1-B og M4-C. Modellene inkluderer nedstrøms skråningsvern utført som plastring med støtte (tåstøtte) for nederste stein. Modelloppsett M4-C representerer en halv dam der plastringen er lagt på nedstrøms støttefylling, mens modelloppsett M1-B representerer kun skråningsvernet der plastringen er lagt på en rampe. Modelloppsett M4-C inkluderer effekt fra både gjennomstrømning og overtopping, mens modelloppsett M1-B utsettes kun for overtopping. Under modellforsøkene er vannføringen gradvis økt inntil brudd inntreffer. Modelloppsettene M1-B og M4-C inkluderer måling av laster på tåstøtten. Målt last omfatter del av plastringen sin egenvekt samt hydraulisk last fra overtoppingsvannføringen. Forskyvninger i plastringen er målt med laser. I tillegg ble 3D endringer undersøkt med fotogrammetri og bruk av metoden Structure-From-Motion for modelloppsett M4-C.

Det er gjort en sammenligning og evaluering på tvers av ovennevnte modelloppsett samt lignende oppsett med skråningsvern utført som plastring uten tåstøtte og skråningsvern av rauset stein (røysfylling). Resultatene er diskutert, og blant annet er vannføring og lastverdier sett i sammenheng med anbefalinger i NVE sin veileder for fyllingsdammer. Rapporten viser at det er tydelig sammenheng mellom forskyvninger av stein i plastringen, aksiale lastverdier målt ved damtåa og overtoppingsvannføring. Den viser også betydningen av vanngjennomstrømning i støttefyllingen.

Stability evaluation of toe supported ripraps exposed to overtopping

NVE Project nr. 80418

Théo Dezert
Fjóla G. Sigtryggsdóttir

Department of Civil and Environmental Engineering
Norwegian University of Science and Technology
Trondheim, June 2022

NTNU
Norwegian University of Science and Technology

NVE

Abstract

Rockfill dams are hydraulic structures that can be exposed to extreme flood events, in turn leading to overtopping. These phenomena erode and affect structural and geotechnical integrity, which can induce dam breaching. Ripraps are broadly used for rockfill dam protection against such erosion processes. Understanding the riprap behavior during overtopping is an important issue to improve dam design and reinforcement techniques. Two new models (M1-B and M4-C) are presented in this report, aimed at focusing on placed riprap resistance and deformation against overtopping events.

For M1-B model, datasets are obtained from 5 experimental tests while for M4-C models, datasets are obtained from 4 experimental tests. Both models consist of placed riprap built on a rock filter layer in a flume, at the hydraulic laboratory of the Norwegian University of Science and Technology, Trondheim. The riprap stones were placed in an interlocking pattern with a metallic support at the toe. The difference between M1-B model and M4-C model lies in the fact that the riprap and filter layers are lying on a rockfill shoulder in M4-C model while they are lying on a ramp for M1-B model, where no throughflow can occur. The models were subjected to successive and incremental overtopping discharges until their complete failure.

A laser traverse system was used to measure the coordinates (3D) of individual marked riprap stones between each discharge increase and six load cells were located at the toe to measure the imposed loads during the entire procedure. From the total load values, two different types of load contributions could be distinguished: the self-weight of the stones and the hydraulic load depending on the discharge level of the overflow. For M4-C models, 3D models of the dam were also carried out using Structure from Motion technique. This report highlights, the strong relation between riprap stone displacements, axial reaction load values measured at the toe and overtopping discharges as well as the importance of throughflow mechanisms in the rockfill shoulder. Moreover, as demonstrated in previous works, a buckling deformation of the riprap layer was observed and described for both M1-B and M4-C models. The results demonstrate that as the hydraulic load induces 2D deformations of the riprap, a larger part of the riprap weight is supported at the toe. Thus, the measured axial load during overtopping arises both from the hydraulic load and from the load imparted due

to the compaction of the riprap layer. This compaction effect induces an even greater load than the one imposed due to the hydraulic contribution.

The discharge and load results from both M1-B and M4-C models are finally put into perspective with the Norwegian Water Resources and Energy Directorate recommendations for full scale dams and suggest the great resistance of supported riprap at the toe.

Table of contents

PhD thesis that are a part of the research projects at NTNU

Priska H. Hiller (2017). Riprap design on the downstream slopes of rockfill dams,. *Doctoral Thesis, Norwegian University of Science and Technology, Trondheim*.

Ganesh H.R. Ravindra (2020). Hydraulic and structural evaluation of rockfill dam behavior when exposed to throughflow and overtopping scenarios. *Doctoral Thesis, Norwegian University of Science and Technology, Trondheim*.

MSc and Project thesis that are a part of the research projects at NTNU

A. 2017- 2022.

Guri Holte Veslegard (2017): *Plastring av fyllingsdammer - Modellforsøk, praktiske forhold og avvik fra regelverk,* (Master project).

Kofi Ntow Opare (2018) *Load measurements at riprap toe* (Master thesis).

Malin Fossum Asbølmo (2019) *Kartlegging av nedstrøms damtå på valgte fyllingsdammer/Field survey of downstream dam toes on selected rockfill dams* (Master project).

Malin Fossum Asbølmo (2019) *Utforming av damtå og betydning for plastring av fyllingsdammer - Kartlegging og modellforsøk/ Significance of toe support conditions on placed riprap stability- Field survey and model studies* (Master thesis).

Nils Solheim Smith (2020) *Physical and numerical modelling of extreme flow through rockfill dams* (Master thesis).

Styrmir Sigurjonsson (2020) *Breaching of rockfill dams* (Master thesis).

Ghaith Alkholossi (2021) *Rockfill dam breaching experiments with the application of photgrammetry techniques* (Master thesis)

Nisal Deelaka Halaba A. Senarathna (2021) *Effect of downstream erosion protection on the breaching of rockfill dams* (Master thesis).

Raj Kumar Kc (2022) *Experimental study into the overtopping and breaching of rockfill dams with erosion protection* (Master thesis).

Saroj Sapkota (2022) *Overtopping and breaching of rockfill dams with and without a central core* (Master thesis).

B. 2014-2016.

Ellen Bogfjellmo (2013): *Nedstrøms skråning av steinfyllingsdammer - Analyse av eksisterende plastringer. Development of a method to survey placed riprap on rockfill dams,* (Semester project).

Hans Edward Røer (2014): *Nedstrøms skråning av steinfyllingsdammer - Modellforsøk av plastring under ulike strømningsforhold. Scaled model tests of placed riprap exposed overtopping, through flow and a combination*, (Master thesis).

Ragnhild Sørlie Meaas (2014): *Plastring av elvebunn med sterk strøm. Scaled model tests of placed riprap exposed to supercritical flow,* (Master thesis).

Johannes Kobel (2014): *Smartstones. Testing out the Smartstone sensors and evaluate its application properties,* (Semester project).

Jens Jakobsen (2015): *Plastring av fyllingsdammer - Forskyving i plastring og anvendelse av Smartstone sensorer. Evaluating displacements in placed riprap and test the application of the Smartstone sensors,* (Master thesis).

Eirik Helgetun Pettersen (2015): *Plastring av fyllingsdammer - Effekt av forband på styrken av plastringen. The effect of interlocking placement on the stability of placed riprap,* (Master thesis).

Wiebke Marie Zander (2015): *Untersuchungen zur Genauigkeit von Smartstones - ein auf RFID-Technologie basierendes Tracersystem. Evaluating the accuracy of the Smartstone - a tracer system based on RFID technology,* (Bachelor thesis).

Fredrikke Kjosavik (2015): *Plastring av fyllingsdammer - Forskyvingar i damkrona. Analysis of displacements on the dam crest with large-scale field tests and scaled model tests,* (Master thesis).

Guri Holte Veslegard (2016): *Plastring av fyllingsdammer - Forskyving i plastring. Analysis of displacements within placed riprap,* (Semester project).

List of papers published as a part of the research projects at NTNU

A. 2018-2022

1. **Buckling analogy for 2D deformation of placed ripraps exposed to overtopping.** Ravindra, G.H.R., Sigtryggsdottir, F.G and Lia, L (2020). *Journal of Hydraulic Research,* DOI: https://doi.org/10.1080/00221686.2020.1744745.
2. **Toe support conditions for placed ripraps on rockfill dams- A field survey.** Ravindra, G.H.R., Sigtryggsdottir, F.G., Asbølmo, M.F and Lia, L (2019). *Vann* 2019 (3), pp. 185- 199. Retrieval link: https://vannforeningen.no/dokumentarkiv/toe-support-conditions-for-placed-ripraps-on-rockfill-dams-a-field-survey/
3. **Failure mechanism in placed riprap on steep slope with unsupported toe.** Ravindra, G.H.R., Gronz, O., Dost, B and Sigtryggsdottir, F.G. *Engineering Structures* 2020, Volume 221. DOI: https://doi.org/10.1016/j.engstruct.2020.111038
4. **Non-linear flow through rockfill embankments.** Ravindra, G.H.R., Sigtryggsdottir, F.G and Høydal, ØA (2019). *Journal of Applied Water Engineering and Research,* 7:4, 247-262. DOI: https://doi.org/10.1080/23249676.2019.1683085
5. **Effects of toe configurations on throughflow hydraulic properties of rockfill embankments.** Kiplesund, GH., Ravindra, G.H.R., Rokstad, M.M and Sigtryggsdottir, F.G (2021)**.** *Journal of Applied Water Engineering and Research*. DOI: https://doi.org/10.1080/23249676.2021.1884615
6. **Laboratory Investigations into Stability and Breaching of Rockfill Dams** Kiplesund, GH., Ravindra, Sigtryggsdottir, F.G (2021) *Publications of the Institute of Geophysics, Polish Academy of Sciences, C.*
7. **Numerical Modeling of the Effects of Toe Configuration on Throughflow in Rockfill Dams.**

Smith, N.S.; Ravindra, G.H.R.; Sigtryggsdottir, F.G.. (2021) *Water. vol. 13 (13).* DOI : https://doi.org/10.3390/w13131726

8. **Placed Riprap Deformation Related to Axial Load at Toe Support: Physical Modelling.** Dezert, T., Ravindra, G.H.R., Sigtryggsdóttir, F.G. (2022), In *Water*, *14*, 1581. *Water. 13(13), 1726.* DOI: https://doi.org/10.3390/w14101581
9. **Evaluation of design criteria for downstream riprap of rockfill dams.** Ravindra, G.H.R., Sigtryggsdottir, F.G., Lia, L (2018), Q. 101- R.71, pp. 1195- 1209, Twenty- sixth International Congress on Large Dams, 4th- 6th July, Vienna, Austria, Published by CRC Press, Taylor and Francis Group.
10. **Protection of embankment dam toe and abutments under overtopping conditions.** Ravindra, G.H.R., Sigtryggsdottir, F.G., Lia, L (2018), 3rd International Conference on Protection against Overtopping, 6- 8 June, Grange over Sands, UK.
11. **Stability and failure mechanisms of riprap on steep slopes exposed to overtopping**. Hiller, P.H., Ravindra, G.H.R (2020), In: Zhang JM., Zhang L., Wang R. (eds) Dam breach modelling and risk disposal. ICED 2020, Springer series in Geomechanics and Geoengineering. Springer, Cham.
12. **Riprap Protection Exposed to Overtopping Phenomena: A Review of Laboratory Experimental Models** Dezert, T., Kiplesund, G. H., & Sigtryggsdóttir, F. G. (2022). Water, 14(17), 2722.
13. **Pertinence of parametric based breach models for rockfill dams.** Sigurjónsson, S., Sigtryggsdóttir, F.G., Kiplesund, G. (2022), Proceedings of the 20th Int. Conf. On Soil Mechanics and Geotechnical Engineering, Sydney 2021.
14. **Riprap and rockfill dam experimental models exposed to overtopping events.** Dezert, T., Ravindra, G.H.R., Sigtryggsdóttir, F.G. (2022), 27th ICOLD congress in Marseille, France, May 2022.
15. **Physical and numerical research on rockfill dams subjected to throughflow due to core overtopping.** Smith, N.S.; Kiplesund, G.H.; Ravindra, G.H.R.; Rokstad; M.M., Sigtryggsdottir, F.G. (2022), 27th ICOLD congress in Marseille, France, May 2022.
16. **Load and deformation relations of placed riprap model with toe support.**

Dezert, T., Ravindra, G.H.R., Sigtryggsdóttir, F.G. (2022), 39th IAHR congress in Granada, Spain, June 2022.

17. **Laboratory investigations into stability and breaching of rockfill dams using dynamic Structure From Motion.**
Kiplesund, G.H., Sigtryggsdottir, F.G. (2022), 39th IAHR congress in Granada, Spain, June 2022.

B. 2014-2018

1. **Accumulating stone displacements as failure origin in placed riprap on steep slopes.**
Priska H. Hiller, Jochen Aberle, *Journal of Hydraulic Research*, 2018, DOI: http://dx.doi.org/ 10.1080/ 00221686.2017.1323806
2. **Field and model tests of riprap on steep slopes exposed to overtopping.** Priska H. Hiller, Leif Lia, Jochen Aberle, *Journal of Applied Water Engineering and Research, 2018*. DOI: https://doi.org/10.1080/23249676.2018.1449675
3. **Smartstones: A small 9-axis sensor implanted in stones to track their movements.**
Oliver Gronz, Priska H. Hiller, Stefan Wirtz, Kerstin Becker, Thomas Iserloh, Manuel Seeger, Christine Brings, Jochen Aberle, Markus C. Casper, Johannes B. Ries (2016) *CATENA*: 142, 245-251, Doi: http:// dx.doi.org/ 10.1016/ j.catena.2016.03. 030.
4. **Placed riprap as erosion protection on the downstream slope of rockfill dams exposed to overtopping.**
Priska H. Hiller, Leif Lia, *25th Congress on Large Dams Stavanger*, Norway, 2015.
5. **Dam Svartevatn - An example of challenging upgrading of a large rockfill dam.**
Priska H. Hiller, Leif Lia, Per Magnus Johansen, Rolv Guddal*, ICOLD Annual Meeting and Symposium* Bali, Indonesia, 2014.
6. **Riprap design on the downstream slope of rockfill dams.**
Priska H. Hiller, Leif Lia, Jochen Aberle, Stefan Wirtz, Markus C. Casper
Mitteilungen - Leichtweiss-Institut für Wasserbau der Technischen Universität Braunschweig Vol. 161, 39-44, 2014.

7. **Large-scale overtopping tests - Practical challenges and experience**.
   Priska H. Hiller, Leif Lia, *1st International Seminar on Dam Protections against Overtopping and Accidental Leakage,* Madrid, Spain, 2014.
8. **Practical challenges and experience from large-scale overtopping tests with placed riprap.**
   Priska H. Hiller, Leif Lia (2015), In M. Á. Toledo, R. Morán, E. Oñate (Eds.*), Dam Protections against Overtopping and Accidental Leakage*, 151-157. London: CRC Press/ Balkema.
9. **Field tests of placed riprap as erosion protection against overtopping and leakage**.
   Priska H. Hiller, Fredrikke Kjosavik, Leif Lia, Jochen Aberle, *United States Society on Dams - Annual Meeting and Conference Denver* CO, USA, 2016.
10. **Kartlegging av plastring på nedstrøms skråning av fyllingsdammer**. Survey of placed riprap on the downstream slopes of rockfill dams, Priska H. Hiller NTNU Report B1-2016-1, ISBN-10: 978-827598-095-1 Trondheim, Norway, 2016.

List of Figures

List of Tables

1 Introduction

Embankment dams, built with locally excavated rockfill or earth fill materials represent 78% of the total existing dams worldwide (ICOLD). The ones composed of coarse-grained material for over 50% are classified as rockfill dams and stand for 13% of the whole world dam population. There are currently over 360 large dams (over 15 m high) in Norway and over 180 of these are rockfill dams.

Dam safety is essential considering the potential catastrophic consequences of a dam break. Thus, the most common causes of dam failure incidents over the decades have been compiled to identify probable factors which contribute to dam instability. This includes investigations into failure and breaching of embankment dams. ICOLD statistics (ICOLD, 2021) state overtopping as the main cause of embankment dam failure appearing as the primary factor in 40% of the total number of failures. Hence, equipping embankment dams, including rockfill dams, with defense mechanisms to safeguard the dam structure against unanticipated overtopping or leakage events is of importance from a dam safety perspective.

Under overtopping conditions, the downstream slope of a rockfill dam is subjected to highly destabilizing dynamic forces generated due to turbulent throughflow (overtopping of dam core) and or overflow (overtopping of dam crest). Considering throughflow conditions, turbulent flow with high seepage velocities within the embankment structure can result in internal erosion and also destabilize the downstream embankment due to pore pressure build up. Further, under overflow conditions, the downstream slope is inundated with highly turbulent surface flow resulting in preogressive external erosion leading to dam breach.

Ripraps are one of the most widely used erosion protection measures for various in-stream hydraulic structures such as embankment dams, spillways, streambeds, river banks, bridge piers and abutments (e.g. Hiller et al., 2019; Thornton et al., 2014; Abt et al., 2013; Khan & Ahmad, 2011; Siebel, 2007). Ripraps are also used in coastal protection structures such as dikes, embankments and jetties against wave action (Kobayashi & Jacobs, 1985). As applied to rockfill dam engineering, ripraps are constructed on the upstream embankment to protect against erosion resulting because of wave impacts and ice induced forces. Further, ripraps

are constructed on the downstream slope to protect against erosion due to accidental leakage or overtopping events.

In the field, two main types of riprap structures can be encountered on rockfill dams: dumped riprap and placed riprap. The difference between these two structures lies in the construction technique. While dumped riprap are composed of stones placed randomly on the dam shoulder, placed riprap correspond to an arrangement of stones that follow an interlocking pattern. Owing to this specific arrangement, placed riprap is more resistant against overtopping events (Hiller et al., 2018; Ravindra et al., 2020) even though setting up such structures remains more expensive than dumped riprap from an economic standpoint.

Abt and Thornton (2014) detailed the advances in research on riprap design for overtopping, mentioning important authors and works such as Siebel (2007), Olivier (1967), Stephenson (1979), Abt and Johnson (1991) and Khan and Ahmad (2011), and many more. Moreover, Najafzadeh and Oliveto (2020) used experimental datasets from many authors to assess the performance of artificial intelligence techniques to predict critical overtopping discharge values for riprap failure. Their results demonstrate that the stone-related Froude number is mainly controlled by the dam slope. However, most of these works only display research on dumped riprap on moderate slopes ($S < 0.5$). As detailed in Ravindra (2020), failure mechanisms differ a lot from dumped to placed riprap exposed to overtopping, especially if they are supported at the toe. Therefore, it is important to also consider scientific publications on placed riprap design with toe support such as Hiller et al., (2018), Knauss (1979), Larsen et al., (1986), Sommer (1997), Dornack (2001), Peirson et al., (2008), Ravindra et al., (2021).

Being able to detail and understand the rupture mechanisms of the exposed riprap to overtopping is of importance since these events are responsible for most structural failure cases (Jandora and Říha, 2008). Moreover, a better understanding could help improving the construction and reinforcement techniques of ripraps.

This report is dedicated to the evaluation of toe supported riprap exposed to overtopping from data acquisition on experimental models. For a pertinent and complete state of art on stability of placed ripraps and on the hydraulic response of rockfill dams under overtopping conditions, we refer the readers to the previous NVE Ekstern rapport nr. 17/2021 (Ravindra and Sigtryggsdóttir, 2021) where detailed information can be found in Section 3.

1.1 Research at NTNU

Experimental and analytical studies on rockfill dams subjected to throughflow and overtopping been conducted at the Department of Civil and Environmental Engineering at NTNU, Trondheim, for over a decade. The work has been carried out in two main research projects, starting with PlaF in 2013 (Development of a tool for optimal riprap protection of rockfill dams) and continued in 2017 in the research center HydroCen within project WP1.2 Dams and dam safety. NVE Ekstern rapport nr. 17/2021 (Ravindra and Sigtryggsdóttir, 2021) summarizes main findings from these two research projects with work conducted from 2014 to 2020. The present technical report presents further results from these research projects as well as new experimental work carried out in 2022.

The master theses and PhD theses associated with the above mentioned research projects are listed on page 5 to 12, along with journal publications and conference articles. The PhD thesis within these research projects are those of Priska H. Hiller in PlaF and Ganesh H.R. Ravindra in WP1.2 HydroCen (A1.2.1). Additionally, publications that are a part of the ongoing PhD work of Geir Helge Kiplesund in WP1.2 HydroCen (A.1.2.2) are listed, as well as publications relating to ongoing postdoctoral project in WP1.2 HydroCen of the first author of this report, Théo Dezert.

Professor Leif Lia was Priska H. Hillers supervisor, and Professor Jochen Aberle was her co-supervisor. Fjóla G. Sigtryggsdóttir was Ganesh H.R. Ravindra's main supervisor and Prof. Leif Lia his co-supervisor. They are also supervisors for Geir Helge Kiplesund. Professor Fjóla G. Sigtryggsdóttir is the project manager for project WP1.2 Hydrocen.

2 Scope and objective of this present report

Many experimental and analytical studies conducted at the Department of Civil and Environmental Engineering at NTNU (Trondheim) have been directed towards investigating failure mechanisms in rockfill dam models subjected to throughflow and/or overtopping conditions. This present report, as a continuation of the previous NVE Ekstern rapport nr. 17/2021 from Ravindra and Sigtryggsdóttir (2021), aims at achieving a better understanding of hydraulic and structural response of placed riprap layer supported at the toe, under extreme loading circumstances.

First, a summary of research methods and experimental model previously carried out in the hydraulic laboratory (NTNU, Trondheim) are introduced in **Chapter 3** of this technical report.

Then, in **Chapter 4**, analysis and results from data acquired on an experimental model in 2018 are displayed. They deal with the behavior of riprap layer built on a ramp and exposed to overtopping, with focus on the support condition at the downstream riprap toe. Experimental data is analyzed, including loads measured at the toe and 2D riprap stone displacements. The Chapter 4 bases on the work presented by Dezert et al. (2022).

Chapter 5 introduces new physical model with tests that have been carried out in spring of 2022. This chapter aims to display the models as well as the types of measuring devices and data acquisition. Experimental data is analyzed, and riprap displacement is studied from 3D models built using Structure from Motion technique. The Chapter 5 bases on the work presented by Dezert and Sigtryggsdóttir (2023).

Chapter 6 evaluates the research findings and compare the scaled laboratory results from chapters 4 and 5 with NVE recommendations.

Finally, a discussion is provided in **Chapter 7** to go deeper into the interpretation of the results from the experimental tests, to point out the potential limitations and to propose some recommendations. This chapter also aims at putting into perspectives the obtained results from these two new studies with the other previous tests carried out at the hydraulic laboratory.

The present report is prepared in compliance with a contract between NVE and NTNU on project nr. 80418 in NVE registry, with the Norwegian title “Plastring, damtå og bruddforløp for fyllingsdammer” or “Riprap, dam toe, and breaching of embankment dams”. This report focuses on the riprap and load measurement at the riprap toe. The report is part of a research project at NTNU conducted within WP1.2 HydroCen.

3 Research methods

This chapter is an updated version of Section 4 from the previous NVE Ekstern rapport nr. 17/2021 (Ravindra and Sigtryggsdóttir, 2021).

The main objective of the research project has been the understanding of the behavior of downstream section of rockfill dams when exposed to accidental leakage and/or overtopping events. To achieve this purpose, many experimental models with overtopping test as well as large-scale field studies have been carried out (Figure 1). Each of these models were built from knowledge acquired during previous investigations. Even though only two models are detailed in this report (**Chapters 4** and **5**), a short overview of the 5 activities within the research project is listed below:

Activity 1: Model 1 *(M1)*- Riprap model with fixed toe support

1D and 2D descriptions of failure mechanisms in placed ripraps.

Activity 2: Field survey 1 *(FS1)*- Large-scale field study of ripraps

Documentation of existing state of riprap toe construction on Norwegian rockfill dams.

Activity 3: Model 2 *(M2)*- Riprap model with unrestrained toe

Riprap stability investigations with realistic toe support conditions**.**

Activity 4: Model 3 *(M3)*- Rockfill dam models with disparate toe configurations

Presenting quantitative descriptions of effects of toe configurations on throughflow hydraulic properties of rockfill dams.

Activity 5: Model 4 *(M4)*- Rockfill dam models coupled with riprap and toe structures

Evaluation of holistic stability aspects of rockfill dam structure coupled with riprap and internal toe.

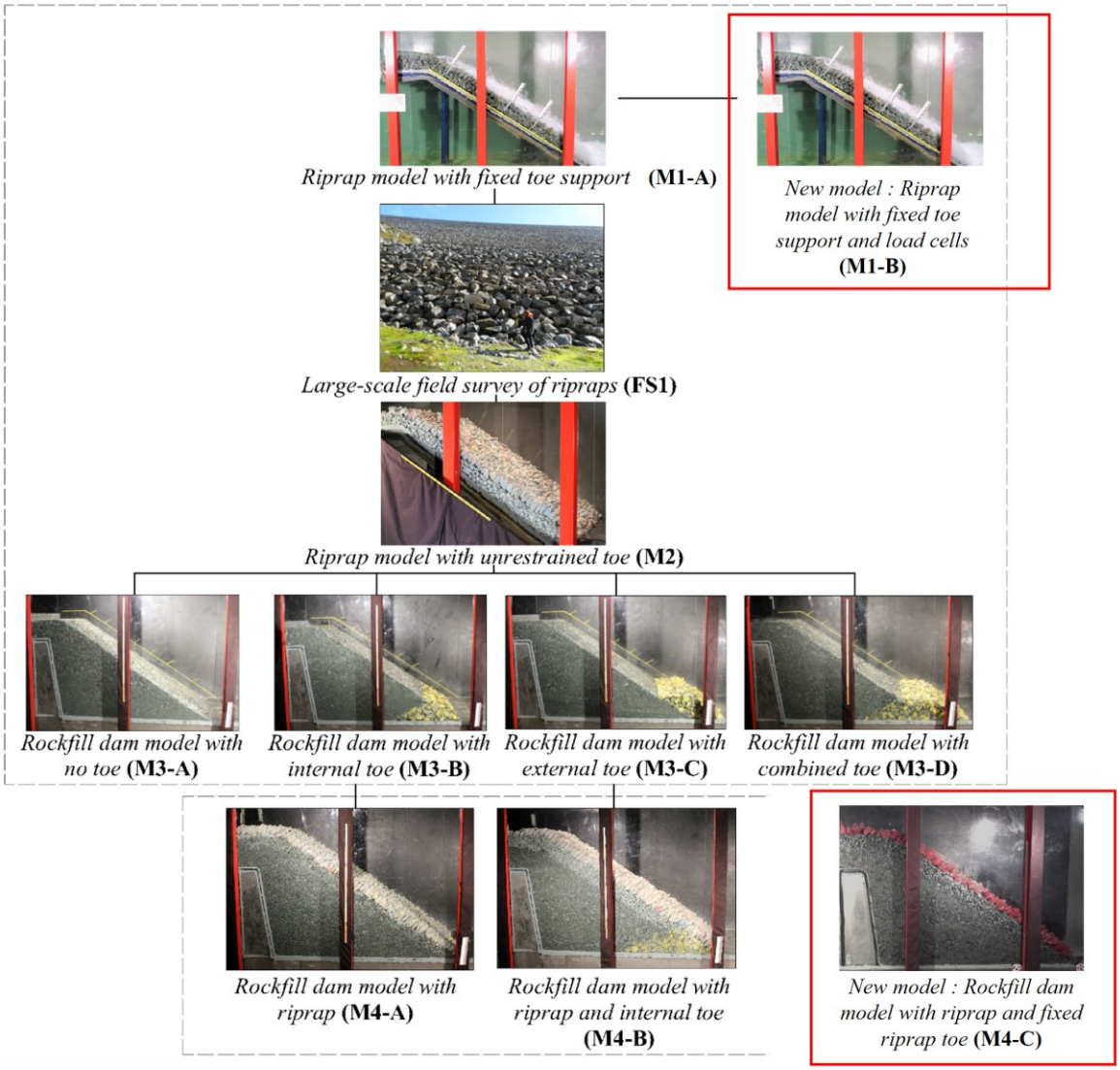

Figure 1. Overview of model tests and field studies conducted as a part of the research program. M1-B and M4-C are the new models setup for the present report. Updated from Ravindra and Sigtryggsdóttir (2021).

First, Hiller et al., (2018) described the 1D failure process of placed riprap stones on a ramp, exposed to successive overtopping, and with a support at the toe section (M1-A). Ravindra et al., (2019) then conducted a field survey (FS1) to investigate construction aspects of placed ripraps on rockfill dams. After, Ravindra et al., (2021) focused on understanding the displacement of riprap stones (2D) according to the overtopping water discharge level and the sliding failure mechanism of ripraps unsupported at the toe (M2). They displayed the existence of a deformation of such riprap layer that could be compared to the buckling deformation of a slender-long column, free at one end and maintained at the other. With M3 models, a new step forward was made with the building of rockfill dam models to study the

effects of toe configuration on throughflow properties (Kiplesund et al., 2021). Finally, M4-A and M4-B models were built up to enhance the effect of throughflow within rockfill dam models protected by a riprap layer (Ravindra and Sigtryggsdóttir, 2021). The load sensor measurements of the M1-B, discussed in this report, were not included in the NVE report by Ravindra and Sigtryggsdóttir (2021). However, they were recently presented in Dezert et al (2022).

Models M1-B and M4-C (Figure 1), respectively within research activities 1 and 5, are the newest models to be investigated. This present report is focused on them. Indeed, they both share a common characteristic: their riprap layer is supported at the toe by a metallic support associated with load sensors. The objective of such data acquisition is to get a better understanding of the dynamic load generation processes at the placed riprap toe during overtopping events. This could be considered as an important physical parameter influencing placed riprap stability. Also, the ability to quantitatively predict the forces generated at the toe could improve the design of efficient toe support. Data from M1-B and M4-C models are displayed and discussed in this report. An overview of the models, acquisition procedure and critical loads and discharges are introduced in this report.

4 Riprap with fixed toe support and load cells (M1-B)

This chapter is an adapted version of Dezert et al. (2022).

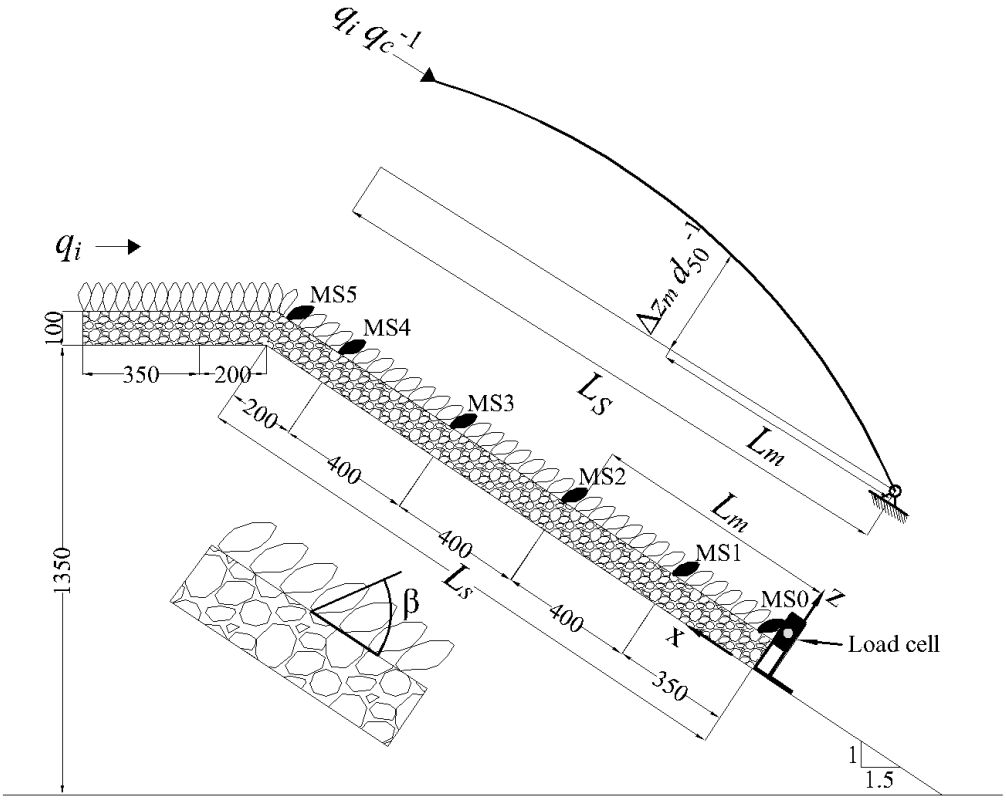

Figure 2. Representation of the experimental set-up with positions of marked riprap stones (MS 0−5) and lengths, adapted from Ravindra et al., (2021).

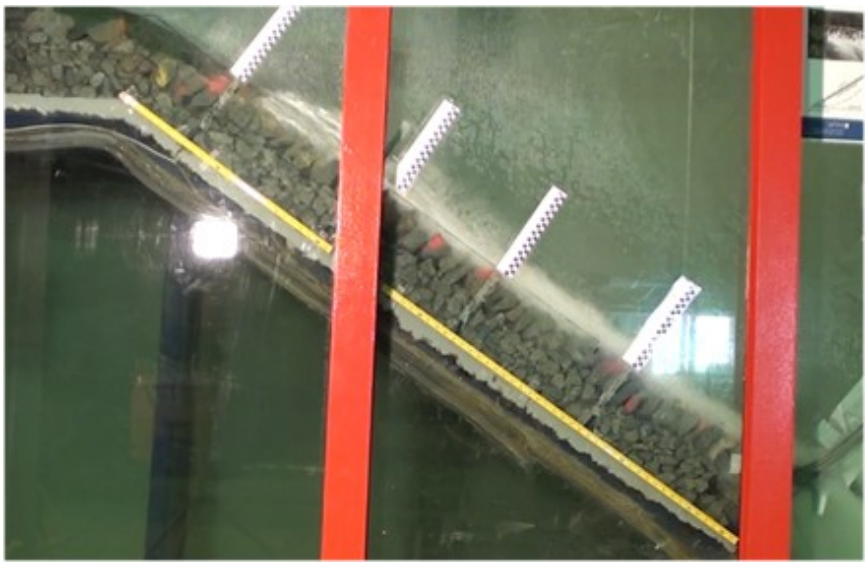

Figure 3. Picture of the experimental model during overtopping.

M1-B models consist of five similar models as the ones built in Hiller et al., (2018) and Ravindra et al., (2021). Also, the same experimental procedure of overtopping is considered. Although, in addition to the laser system used to record the displacement of individual stones, six load cells were added on the metallic toe support structure to measure axial load values during the construction and the experimental testing phases. In this report, one of the objectives is to understand the relation between axial loads measured at the toe, 2D riprap stone displacements, and overtopping water discharge levels on a placed riprap model with toe support. Another goal is to explain the different contributions of the total loads measured at the toe, from the water contribution and from the self-weight of the riprap stones. To do so, the experimental model structure, the followed overtopping procedure and the acquisition methods are first introduced. Then, the axial load values recorded during the building of the riprap layer as well as their values during overtopping testing are displayed. Moreover, their relationship with discharge values and individual riprap stone displacements are presented.

4.1 Experimental set-up and methodology

4.1.1 Model

The experimental set-up considered in this report is nearly the same as the ones used in Hiller et al., (2018) and in Ravindra et al. (2021). Thus, for the reader eager to get more details, complement of information can be found in these previous published works as well as in the previous NVE Ekstern rapport nr. 17/2021 (Ravindra and Sigtryggsdóttir, 2021). Still, an overview of the set-up and experimental procedure is introduced in this section. The experimental tests were carried out at the hydraulic laboratory of NTNU, Trondheim in a horizontal flume (25 m long, 2 m high and 1 m wide). The considered model is a 1:10 scale model of a single riprap layer on the downstream section of a dam designed by Hiller et al., (2018), constructed assuming Froude similarity. The riprap layer is built on a filter layer placed on a ramp inclined at 1:1.5 (vertical: horizontal, $S = 0.67$, Figure 2). The elements of the model are placed across the total width of the flume (1 m) and with a total chute length of $L_s = 1.75$ m. The chute length has been slightly shortened compared to previous models (Hiller et al., 2018; Ravindra et al., 2021) to accommodate the load cells at the bottom of the riprap layer. The horizontal crest length remains the same with 0.55 m. A metallic sheet perpendicular to the chute was fixed at the toe section to support the riprap and the complete model was elevated from the bottom of the flume to avoid backwater effects. Indeed, the

aim of this study is only to focus on erosion and rupture of riprap when exposed to overtopping events.

Five tests (A, B, C, D, and E) were carried out with placed ripraps placed on a filter layer composed of a geotextile and a layer (0.1 m thick) of angular stones with nominal diameter of $d_{50,F}$ = 0.025 m and density of $\rho_{s,F}$ = 3050 kg.m^{-3}. The nominal diameter being $d = (abc)^{1/3}$ (Bunte and Abt, 2001), with a, b, and c respectively standing for the longest, intermediate, and shortest axes. The riprap layer consisted of rhyolite stones with nominal diameter of d_{50} = 0.053 m (a = 0.088 m, b = 0.049 m, and c = 0.036 m) and density of ρ_s = 2710 kg.m^{-3}. The riprap layer was built by manually placing approximately 1 100 stones from the toe section to the crest in an interlocking fashion. The riprap stones on the slope were placed with an inclination of $\beta \approx 60°$ (Figure 2) between the a−axis and the chute bottom while the crest stones were placed with $\beta \approx 90°$ (Lia et al., 2013). The dimensioning of the stones comprising the riprap and the filter layers were carried out in accordance with the Norwegian Water Resources and Energy Directorate guidelines (NVE, 2012). Six riprap stones were selected and marked for each test. They were located in the center of the model (with a distance of 0.5 m to both sides of the flume) at the following positions of x = 0, 0.35, 0.75, 1.15, 1.55, and 1.75 m and were identified as MS0, MS1, MS2, MS3, MS4, and MS5 respectively (Figure 2).

As proposed in previous works from Hiller et al., (2018) and Ravindra et al., (2021), the packing factor parameter defined by Olivier (1967) can be considered as:

$$P_c = \frac{1}{N\, {d_{50}}^2} \tag{1}$$

With N defining the quantity of riprap stones per m^2 and d_{50} the median stone dimension. P_c provides information on the density of the placement of riprap stones, so that low P_c values indicate densely packed stones while higher values stand for loosely packed stones. The P_c values for each of the five tests are displayed in Table 1.

Table 1. Discharge range, critical discharge, and packing factor values for each of the five tests.

Test	q_i (l.s^{-1})	P_c	q_c (l.s^{-1})
A	50–225	0.58	225
B	50–325	0.56	325
C	50–200	0.53	200
D	65–350	0.53	350
E	50–150	0.56	150

4.1.2 Overtopping Procedure

The experimental models were exposed to successive overtopping events (Figure 3), starting at an initial discharge ranging between 50 and 65 l.s^{-1}. The pumps supplying discharge to the flume had a combined maximum delivery capacity of q = 400 l.s^{-1}. The models were located far enough from the inflow section to guarantee calm flow conditions upstream. Under overtopping conditions, the models are inundated with laminar flow on the crest and by turbulent surface flow on the downstream slope (Figure 3). After the initial load period, the discharge level q was successively increased with a range of $q = 25{-}40$ l.s^{-1} and maintained constant for a fixed time interval (Δt = 1800 s) until ultimate rupture of the model was achieved. The water flow was stopped between each discharge increment to measure the 3D positions of the marked riprap stones. The critical discharge value q_c corresponds to the value for which a complete failure of the riprap occurs. For each of the five tests, q_c values are displayed in Table 1 and varied over the range $q_c = 150{-}350$ l.s^{-1}. These values can vary according to placement of stones as well as to the skills of the workers.

4.1.3 Measuring Devices and Data Acquisition

Position of the specific marked riprap stones were recorded by employing an automated 3D-traverse laser placed above the model. It allowed their precise positioning in a 3D Cartesian coordinate system with x−axis parallel to the chute and pointing in the upstream direction (Figure 2) and with z−axis perpendicular to the chute. The origin of the system was located

at the toe section and the accuracy of the measurements were about 0.1 mm in *x*-direction and 1 mm in *z*-direction. The displacements were only considered along *x* and *z* axes but not in the *y*-direction. Recording of the positions were completed before each discharge increment.

In this report, the use of 6 load cells (S9M force transducer manufactured by HBM) to record axial load values, F_i, is discussed. These cells were placed at the toe section of the model (Figure 2) and the sensors had a combined capacity of 3.10^3 N. They were positioned between two metallic frames (one fixed and one movable) so that the riprap layer could be directly placed on them and to take into account only the load from riprap stones and not the one from the filter layer (Figure 4). The recording of the data was made possible during the riprap construction and throughout the five tests (between each overtopping and while the water was flowing). The value for which a complete failure of the riprap occurs is called the critical load value, F_c.

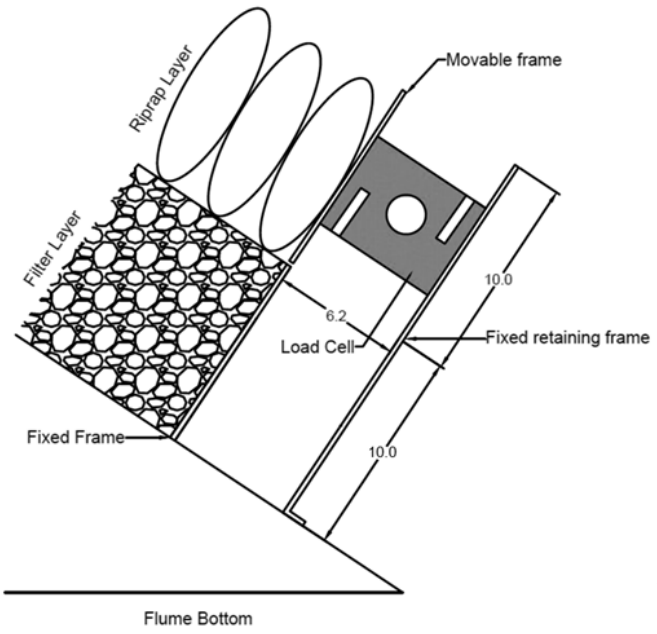

Figure 4. Load cell positioning against the riprap layer between two metallic frames with dimensions in centimeters.

4.2 Data Analysis

The data analysis presented on the M1-B models are based on Dezert et al (2022).

4.2.1 Axial Reaction Loads at Riprap Toe

The axial reaction loads at the toe were monitored while the riprap model was being built, recorded after placement of every 50 stones. These measured values are displayed for each test, according to the length from the toe, in Figure 5. These data highlight that the reaction axial load increases rapidly during the first 0.5 m but then stabilizes to a load value between 100 and 130 N, with test A displaying the greatest axial load values. These data suggest that the weight of the stones have no influence on the axial load at the toe once a certain threshold length is reached.

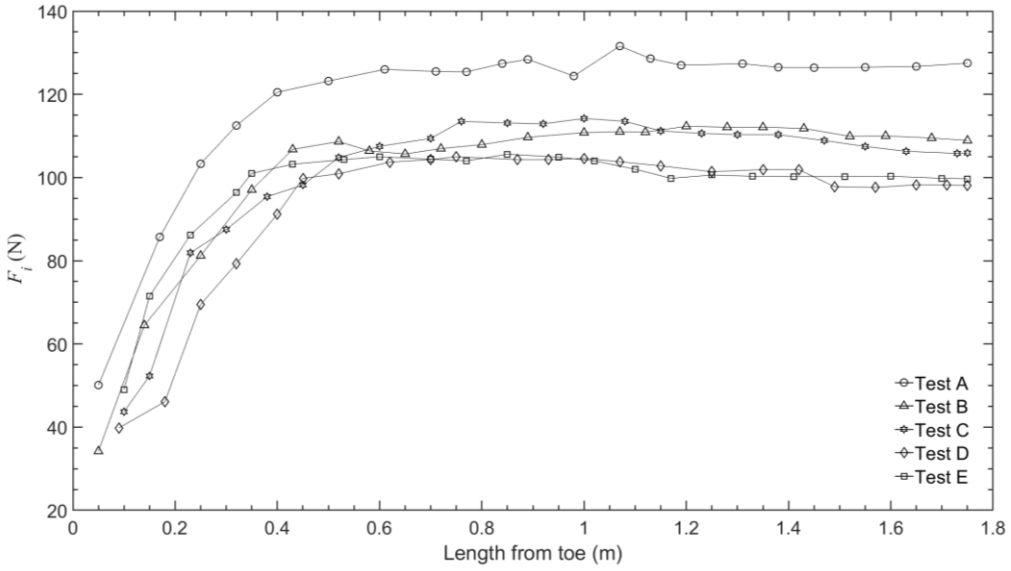

Figure 5. Measured axial load at the toe section of the experimental models during riprap layer building. (Dezert et al., 2022).

After the construction stage and the opening of the pumps, the water flow overtops the model and generates a load increase at the toe section. An example of the load data and discharge values from the pumps for test D is displayed in Figure 6. During overtopping stages, the axial reaction load value F_i was recorded for each test and is displayed in Figure 7 according to discharge value. That axial load then decreases (Figure 6a) when the water flow is stopped between each discharge incrementation (Figure 6b), the stable value reached after cutting off the overtopping flow corresponds to the axial load contribution from the compaction of the riprap, FR_i (Figure 8).

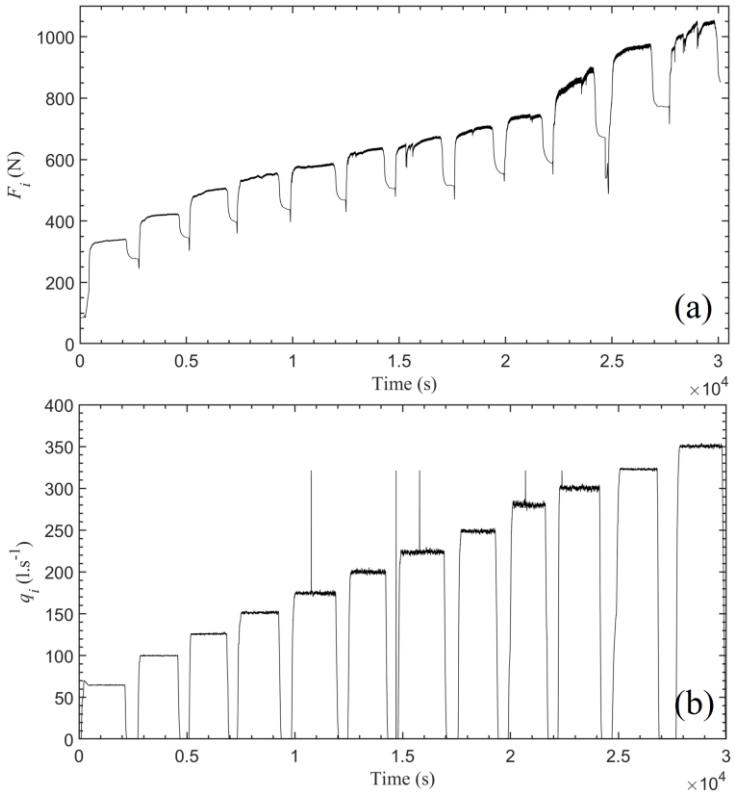

Figure 6. Example of load values (**a**) issued from test D for the six combined cells and associated discharge values (**b**) from the pumps. (Dezert et al., 2022).

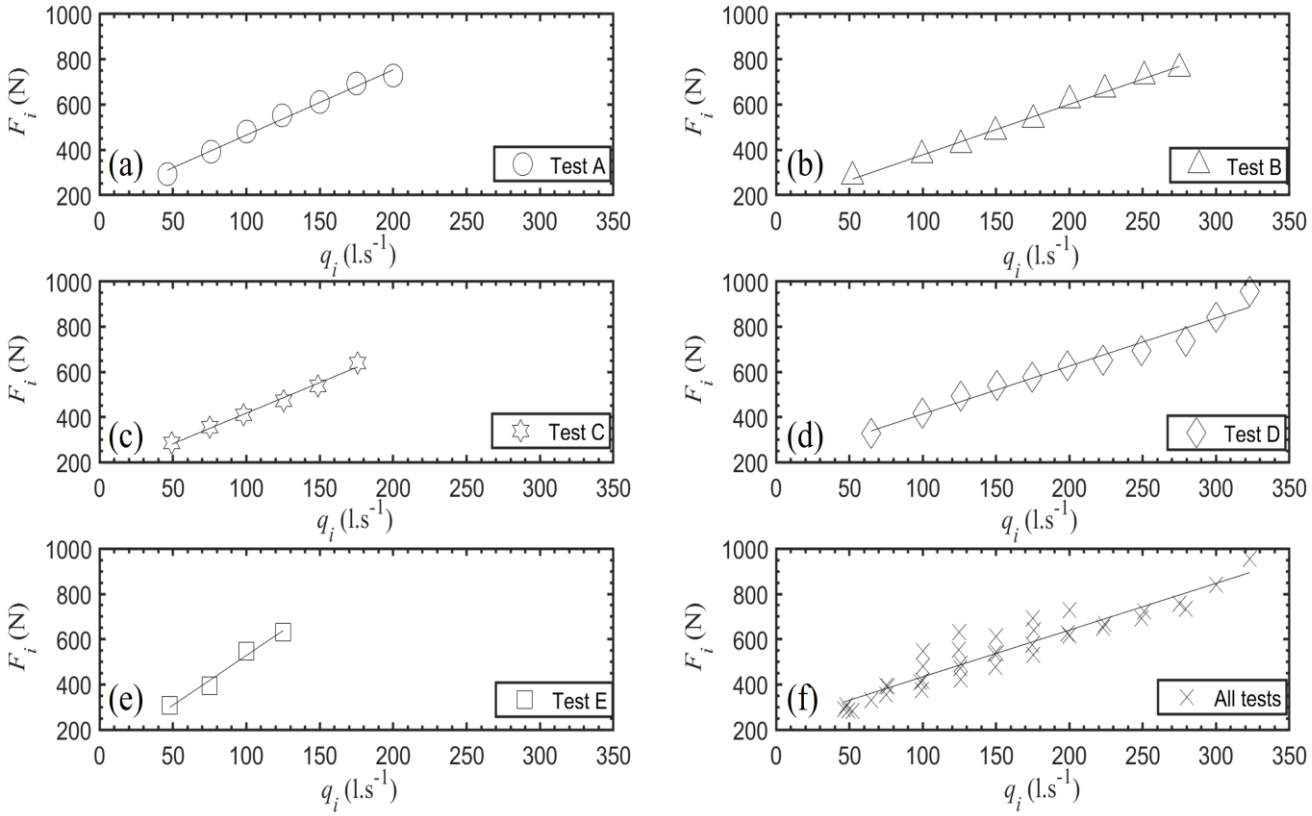

Figure 7. Axial load at the toe section during overtopping event for each of the five tests (**a**−**e**) and for all the tests (**f**) according to discharge values. (Dezert et al., 2022).

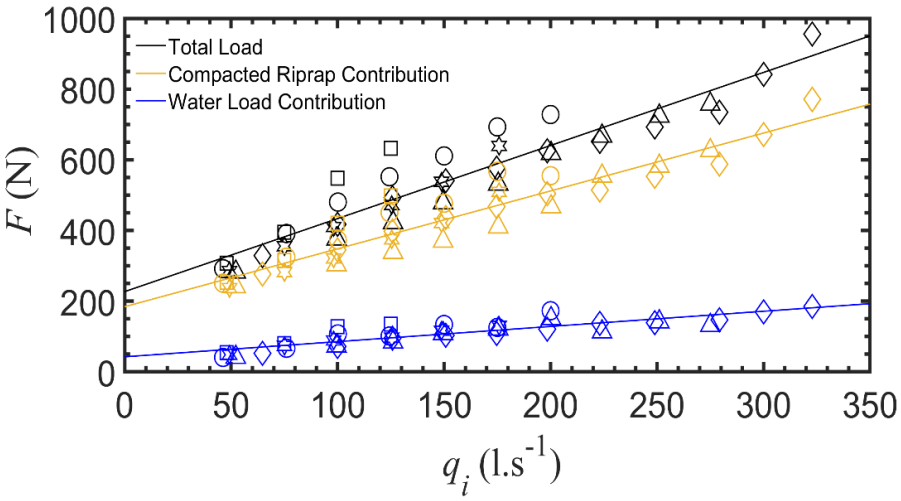

Figure 8. Contribution of the compacted riprap and water loads in the measured total axial load for all tests. The different symbols stand for the five different tests and correspond to the ones displayed in Figure 7 (**a**−**e**). (Dezert et al., 2022).

Figure 7 highlights the strong linear relation existing between axial loads at the toe section and discharge values for individual testing (Nash–Sutcliffe coefficients R^2 close to 1), but also for the complete dataset (R^2 = 0.95) (Figure 7f). A relation (Equation (2)) can thus be proposed to describe the relation between these two parameters:

$$\frac{F_i}{F_c} = 0.77\frac{q_i}{q_c} + 0.226 \quad (2)$$

Even though the axial load at the toe increases along with the discharge rates (Figure 7), Figure 8 displays an increase of the compaction load contribution F_{Ri} (in yellow) between each discharge step break, when no water is flowing over the model. These loads increase after each discharge step and do not come back to their primary value. These data suggest that stone displacement and riprap compaction, imputed to overtopping, induce an increase of the axial load at the toe section. The waterflow contribution F_{Wi} (in blue, Figure 8) appears to have less impact on the axial load at the toe than the compaction load contribution. From Figure 8, it can be observed that $F_i = F_{Ri} + F_{Wi}$.

4.2.2 1D stone Displacements According to Axial Reaction Loads

The displacements of the riprap stones alongside x−axis can be plotted according to axial load values, as it was done by Hiller et al., (2018) and Ravindra et al., (2021) as a function of the applied discharge level. The displacement of individual stones is normalized according

to Larsen et al., (1986) as $\Delta x_m L_m^{-1}$ where $L_m = x_m - x_0$, with m denoting the position of a marked riprap stone along x−axis. The displacement Δx_m corresponds to the difference in stone positions with their initial position before the first overtopping. In Figure 9, the 1D stone displacements were analyzed according to the critical unit load ($F_i\ F_c^{-1}$). As in Ravindra et al., (2021), the stone displacements were considered according to the position of the riprap stone identified as MS0. Indeed, this stone undergoes a moderate displacement since it is maintained by the fixed toe support. The displayed results suggest a good exponential relationship (R^2 ranging from 0.78 to 0.91) between these two parameters, for each test. The respective fitting curves are displayed in black in Figure 9.

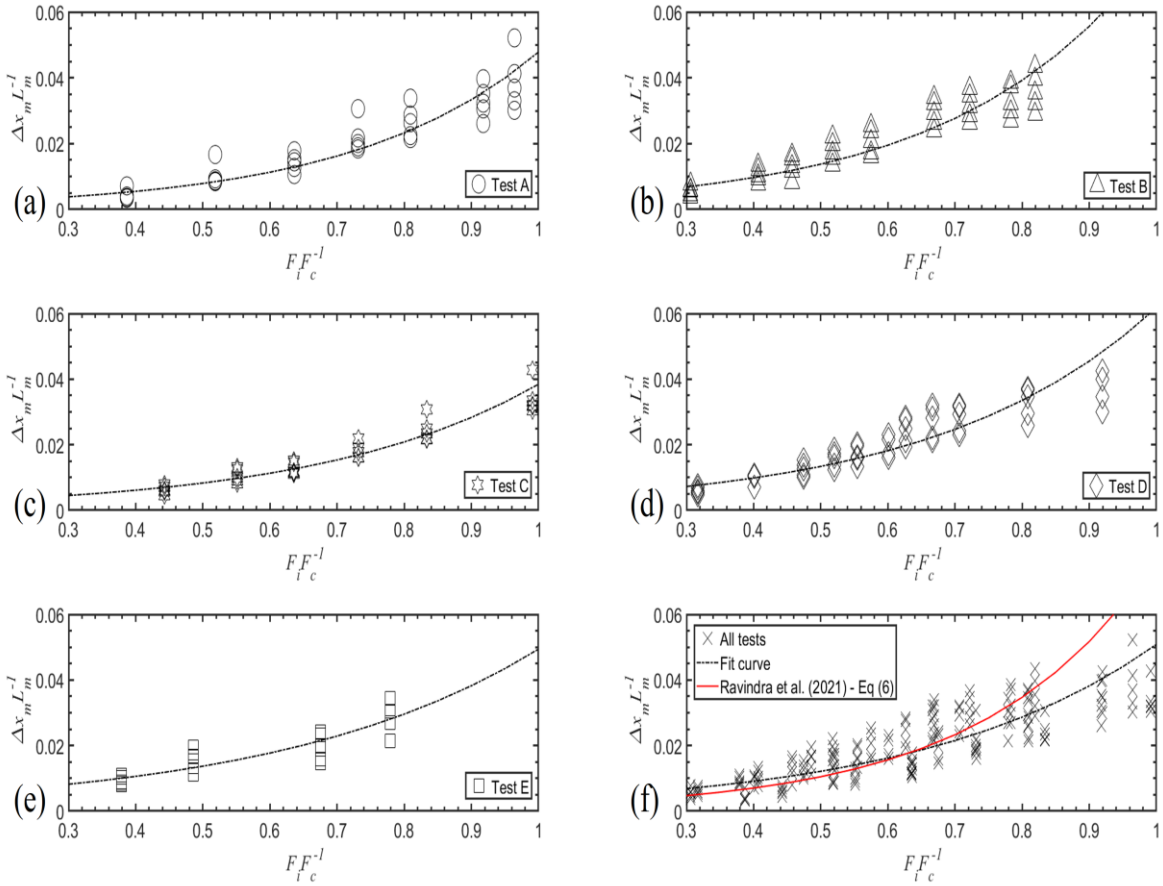

Figure 9. (**a**−**e**) Riprap marked stone displacement along x−axis according to normalized axial load values at the toe section for each of the five tests with exponential fitting curve representation. (**f**) Data for all tests put into perspective with the fitting curve from Ravindra et al., (2021), in red, and the exponential fitting curve for all data, in dotted black line. (Dezert et al., 2022).

The stone displacements along x−axis increase along with the axial load measured at the toe. As a comparison, using the relation between $\Delta x_m L_m^{-1}$ and $q_i\, q_c^{-1}$ proposed in Ravindra et al., (2021) (cf Equation (6) of that report), the respective fitting curve is displayed in red (Figure 9f). This relation was adapted considering the previous relation from Equation (2). It appears that the fitting of this exponential curve is not optimal and the corresponding equation from these data sets (black dotted curve, Figure 9f) should rather be (Dezert et al., 2022):

$$(\frac{\Delta x_m}{d_{50}})_i = 0.0029\, e^{(2{,}86\,\frac{F_i}{F_c})} \tag{3}$$

4.2.3 2D stone Displacements According to Axial Reaction Loads

Owing to the laser measurements, 2D displacements of marked riprap stones could also be computed according to the axial load values measured at the toe of the model. The results from test B data are displayed in Figure 10, with the vertical axis $\Delta z_m d_{50}^{-1}$ standing for the stone displacements along the z−axis (Figure 2) over the nominal stone diameter and the horizontal axis standing for L_m normalized over the total riprap length L_s. They display a progressive displacement in both x and z directions such as the axial load increases. The marked riprap stones tend to go downstream in the x−direction but also to elevate themselves in the z−direction. These displacements are directly related to the magnitude of axial load

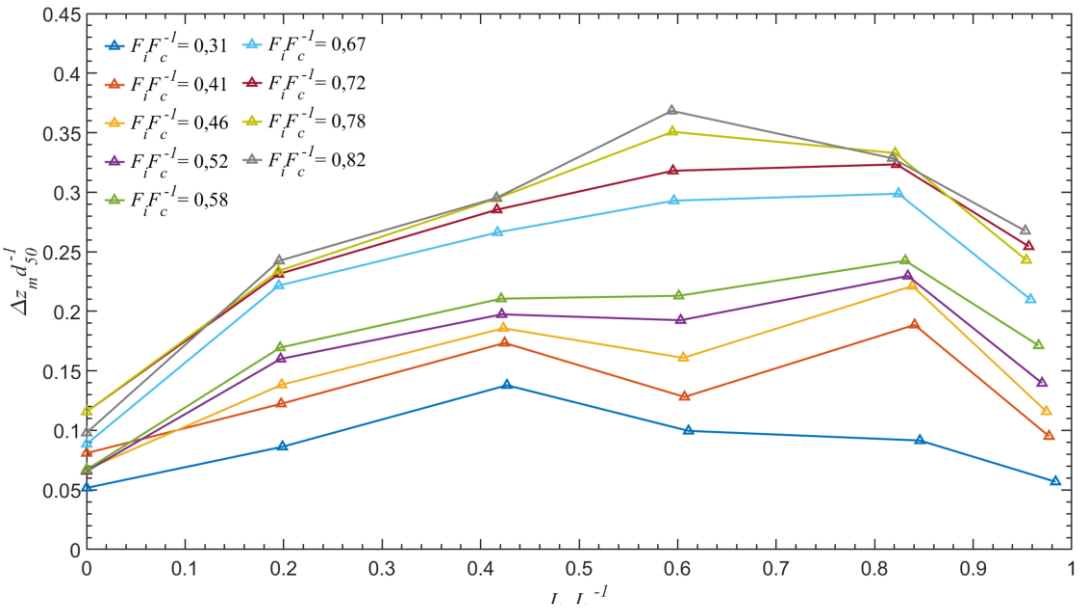

Figure 10. Example of values issued from test B displaying the riprap marked stone displacement along x−axis and z−axis according to normalized axial load values at the toe section. (Dezert et al., 2022).

measured at the toe section. These results are in agreements with the findings from Hiller et al., (2018) and Ravindra et al., (2021). It appears that the magnitude of elevation in the $z-$direction depends on the position of the riprap stone, suggesting a buckling process. The compaction of the riprap layer provokes the creation of a gap at the upstream part of the model. This mechanism combined with the buckling leads to the complete breakage of the structure.

Results from cumulative analysis with data from tests A, B, C, D, and E are displayed in Figure 11, with uncertainty in displacements being shown as 95% confidence intervals. The represented data points are average values for specific $F_i F_c^{-1}$ intervals (0.2−0.4, 0.4−0.6, 0.6−0.8 and 0.8−1). These results attest the ones obtained from Figure 10 (Test B) and echo the one from Ravindra et al., (2021).

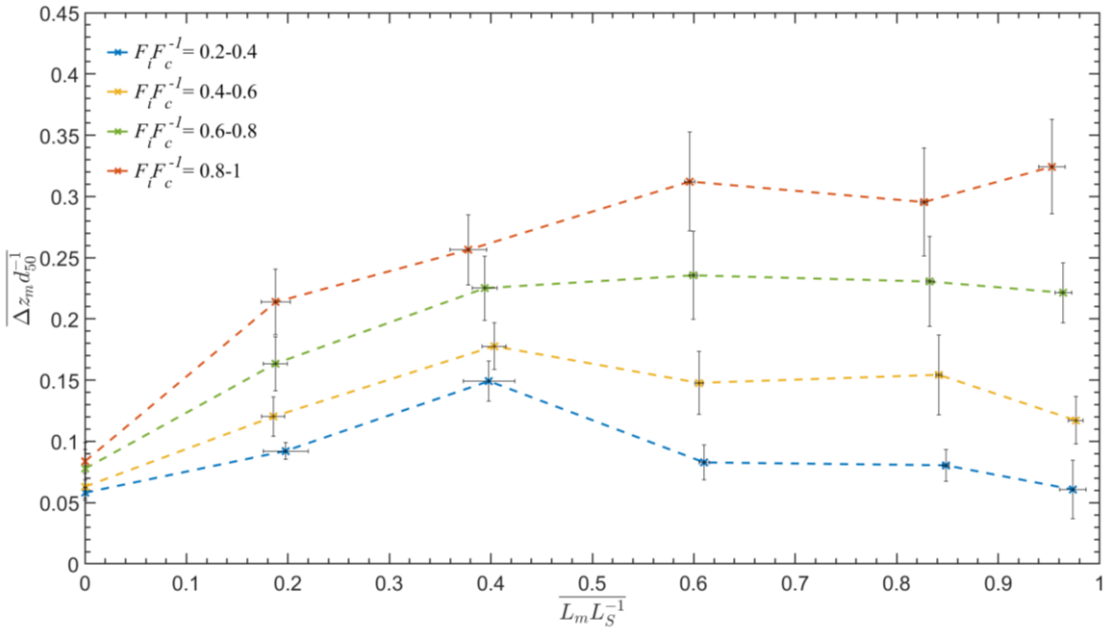

Figure 11. Results of the analysis from the five experimental tests, displaying the average normalized stone displacements along the $z-$axis ($\overline{\Delta_{z_m} d_{50}^{-1}}$) and along the $x-$axis ($\overline{L_m L_S^{-1}}$). The displacements are presented for incremental normalized load values ($F_i F_c^{-1}$) during overtopping. The uncertainties are displayed according to 95% confidence intervals. (Dezert et al., 2022).

From Figure 12, these cumulative results can be compared to the predictive curves obtained by the buckling equation issued from Ravindra et al., (2021):

$$\left(\frac{\Delta z_m}{d_{50}}\right)_i = A\frac{q_i}{q_c}\sin\left(k\pi f\left(\frac{L_m}{L_s}\right)_i\right) \quad (4)$$

With k standing for the buckling mode (k = 1), and A and f parameters for calibration (with respectively A = 0.3 and f = 0.7). Here, Equation (4) is adapted owing to the established relation between axial load and discharge in Equation (2), so that one gets the buckling equation displayed in Equation (5) (Dezert et al, 2022):

$$\left(\frac{\Delta z_m}{d_{50}}\right)_i = \overline{\left(\frac{\Delta z_m}{d_{50}}\right)_{MS0}} + A\left(\frac{\frac{F_i}{F_c} - 0.225}{0.74}\right)\sin\left(k\pi f\left(\frac{L_m}{L_s}\right)_i\right) \quad (5)$$

With $\overline{\left(\frac{\Delta z_m}{d_{50}}\right)_{MS0}}$ the mean relative elevation value of the marked riprap stone *MS*0, equal to 0.0707 in this work. The displayed results are consistent with the ones from Ravindra et al., (2021). It also appears that the fitting of the data is not optimal for smaller loads.

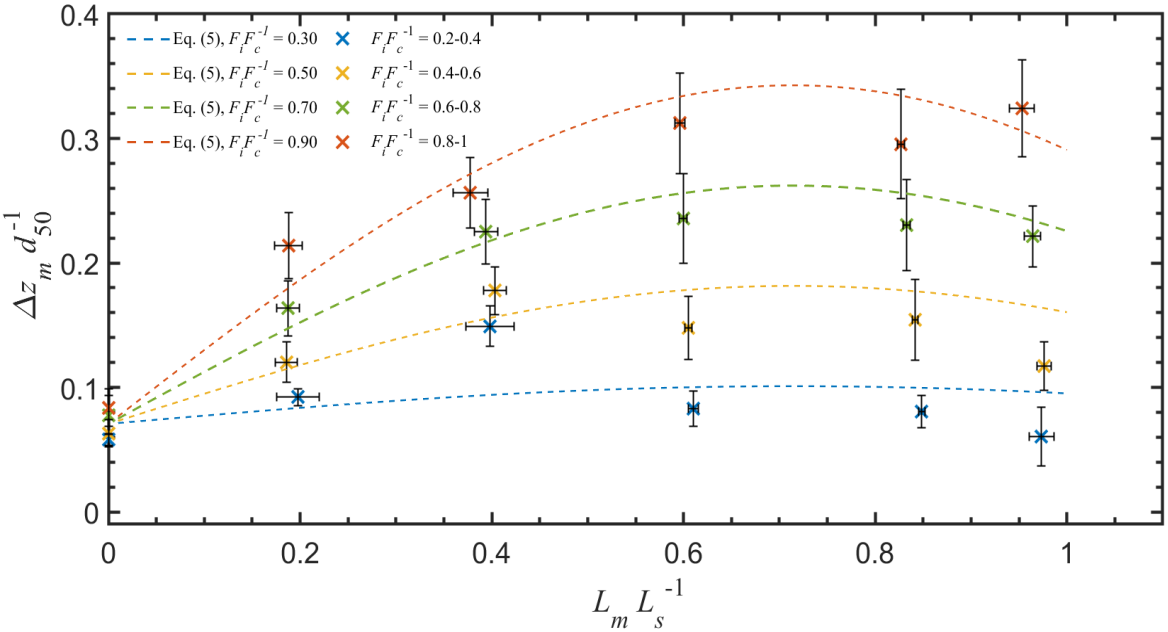

Figure 12. Observed 2D stone displacements from Figure 11 with predicted values from Equation (5) in dotted lines. The average normalized stone displacements are displayed along the z–axis ($\Delta_{z_m} d_{50}^{-1}$) and along the x–axis ($L_m L_s^{-1}$). The displacements are presented for incremental normalized load values ($F_i F_c^{-1}$) during overtopping and the uncertainties are displayed according to 95% confidence intervals. (Dezert et al., 2022).

5 Rockfill dam with riprap, fixed riprap toe support (M4-C)

This chapter is an adapted version of Dezert and Sigtryggsdóttir (2023).

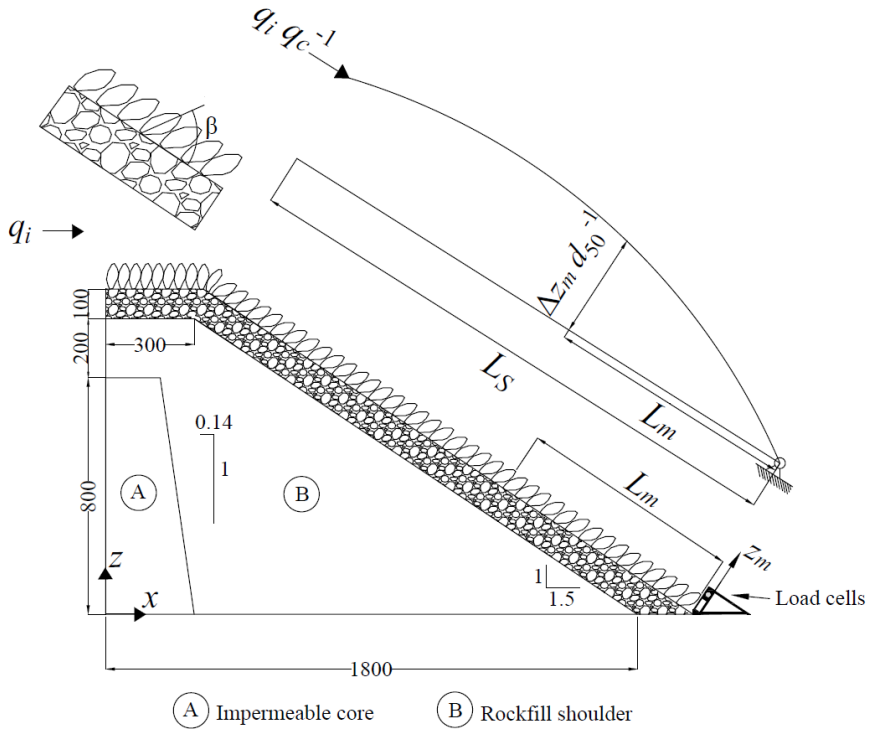

Figure 13. Representation of the experimental set-up of a half dam model with placed riprap layer supported at the toe. Lengths are expressed in millimeters. Dezert and Sigtryggsdóttir (2023).

Figure 14. Picture of the experimental model during overtopping (Test G). Dezert and Sigtryggsdóttir (2023).

A new rockfill dam model (M4-C, see Figure 1) has been set up in the hydraulic laboratory of NTNU (Trondheim) during spring 2022. As M4-A and M4-B models, this new structure consists of a rockfill dam shoulder with a filter layer and placed ripraps on the downstream slope. However, the ripraps were provided with fixed toe supports and load cells, just as the M1-B model (Figure 1). The rockfill dam do not include internal toe, similarly to M4-A model. To demonstrate and to discuss the good repeatability of the testing, the overtopping procedure was executed on 4 models. Such model would help in getting more details concerning interactions between different dam components exposed to overtopping events and understanding their impact on load measured at the toe.

Thanks to the acquired data, we wish to compare the critical discharge value leading to the rupture with the critical discharge values from previous models. We also wish to study the buckling process occurring for supported ripraps, on a dam shoulder instead of a solid ramp. These comparisons are done according to the riprap stone displacements as well as according to the evolution of the measured load at the toe support.

5.1 Experimental set up and methodology

5.1.1 Model

As for all the previous models introduced in this report (Figure 1), the experimental tests for model M4-C were carried out at the hydraulic laboratory of NTNU in the same horizontal flume ($25 \times 2 \times 1$ m^3). The model is a 1:10 scale model of half rockfill dam, as the ones built in Kiplesund et al., (2021).

They consist of a compacted rockfill dam shoulder with well-graded material density of $\rho_{Shoulder} = 2\ 720$ kg.m^3 , coefficient of uniformity of $C_u = 7.5$ and median stone diameter of $d_{50} = 0.0065$ m (area B, Figure 13) with the presence of an impermeable aluminum part standing for the central core (area A, Figure 13). More information on the shoulder material such as grain size distribution can be encountered in Kiplesund et al. (2021). A filter layer and a placed riprap layer were built on the steep downstream slope of 1:1.5 (S = 0.67) with filter material density of $\rho_{Filter} = 3\ 050$ kg.m^3 and median filter stone diameter of $d_{50} = 0.022$ m and with riprap material density of $\rho_{Riprap} = 2\ 600$ kg.m^3 and nominal riprap stone diameter of $d_{50} = 0.057$ m. The nominal diameter can be expressed as $d = (abc)^{1/3}$, with *a*, *b* and *c* respectively standing for the longest, intermediate, and shortest axis. The dimensions of

these models are based on the ones carried out previously in Hiller et al. (2018) and in Ravindra et al. (2021), which consisted of riprap and filter layers built on a ramp without rockfill shoulder, and are based on requirements from the NVE guidelines for embankment dams (Ravindra and Sigtryggsdóttir, 2012). However, a metallic toe support (Figure 13), as previously used in Models M1-B was added to this work. This toe support consists of metallic sheets perpendicular to the chute and supporting only the placed riprap layer, without any contact with the other materials. The dimensions of the models are detailed in Figure 13, they are in the same range as the dimensions of previous models described in Hiller et al., (2018), Ravindra et al., (2021) and Dezert et al., (2022). However, the length of the crest is shorter in this model, with only 30 cm length. Also, the dam model was built on a platform in order to be elevated and to avoid backwater effects.

For this experimental set-up, riprap stones were placed manually on the slope with an inclination of 60° between the *a*-axis and the chute bottom. On the crest, they were placed with an angle of 90° between the *a*-axis and the crest (Figure 13). Within each model, 6 riprap stones were selected and painted in a different colour (yellow) to be distinguishable. These stones were positioned in the center of the model (0.5 m to both sides of the flume) at the approximate following positions : x = 0.5, 0.8, 1.1, 1.4 and 2.05 m with the origin of the system located at the upstream bottom of the core (Figure 13). Four tests (F, G, H, I) were carried out. Though, two different building methods were used for the riprap layer construction. In addition of having their riprap stones placed manually in an interlocking pattern, Tests F and G had their riprap layer packed during construction. Indeed, the workers were stepping on the riprap layer during the construction to reach the top of the model, increasing the compaction of the protective layer. On the other hand, Tests H and I models did not have their placed riprap layer packed since a ladder was positioned above the downstream slope to carefully build the protective layer without putting extra load from the workers on the model. Approximately 1 250 to 1 300 riprap stones were used for the whole layer, according to the building technique and level of packing.

5.1.2 Overtopping procedure

As for M1-B models described in the previous chapter, the M4-C models were exposed to successive overtopping events with an initial discharge of 50 $l.s^{-1}$. After the first loading period, the discharge was successively incremented by 25 $l.s^{-1}$ and kept constant for

Δt =1800 s until breakage of the model. Also, the water flow was stopped between each discharge both to measure the 3D positions of the marked riprap stones and to take picture of the model to build 3D models. During the overflowing of the model, laminar flow is characterized on the crest while turbulent surface flow can be identified on the downstream slope (Figure 14).

5.1.3 Measuring device and acquisition

As for M1-B models, the marked riprap stone positions were recorded thanks to a 3D-traverse laser before each discharge increase. Similarly, 6 load cells were fixed at the toe section of the model. More information can be found in Section 4.1.3 of the present report concerning the laser system and the load cells.

For each of the four models and for every water discharge value, around 50 to 60 pictures were taken before the first overtopping stage and afterwards when the waterflow was stopped, after 30 minutes of overtopping. The photos were taken with a Canon EOS 1300D camera mounting a Canon EFS 18-55 mm lens fixed at 18 mm focal length. From these pictures, without any post-processing, we could carry out the production of 3D models of the dam (Figure 15) with Structure from Motion technique, using Agisoft Metashape software, developed by Agisoft LLC. Here, we are not going deep into the description of Structure from Motion technique but just highlight the main steps. Though, for the reader eager to learn more, detailed information can be found in Agisoft User manual (2021) as well as a descriptive flowchart in Kiplesund et al., (2022), where Structure from Motion technique is used to model an experimental rockfill dam under overtopping condition from video recording.

In this research work, 4 ground control points were used for 3D modelling of the dam. These control points are small white cubes with 1 cm edge, placed at known coordinates around the dam model. Two of them were placed on the sides of the flume, above the crest. The two others were also placed on the sides of the flume but above the toe section. The coordinate system defined in this work is a right-handed XYZ coordinate system with its origin located at the upstream bottom of the core, on the right side of the flume (Figure 15). The structure from motion methodology can essentially be described in 4 main steps : i) loading, removing the unnecessary pictures and aligning the cameras. The alignment consists in matching recognizable features between the pictures (tie points, Figure 15.a) and determining the

position of each camera; ii) building dense point cloud (Figure 15.b) based on the sparse point cloud; iii) building a 3D mesh (polygonal model, Figure 15.c) and a digital elevation model (DEM, Figure 15.e); iv) generating textures on the 3D model and generating an orthomosaic (Figure 15.d).

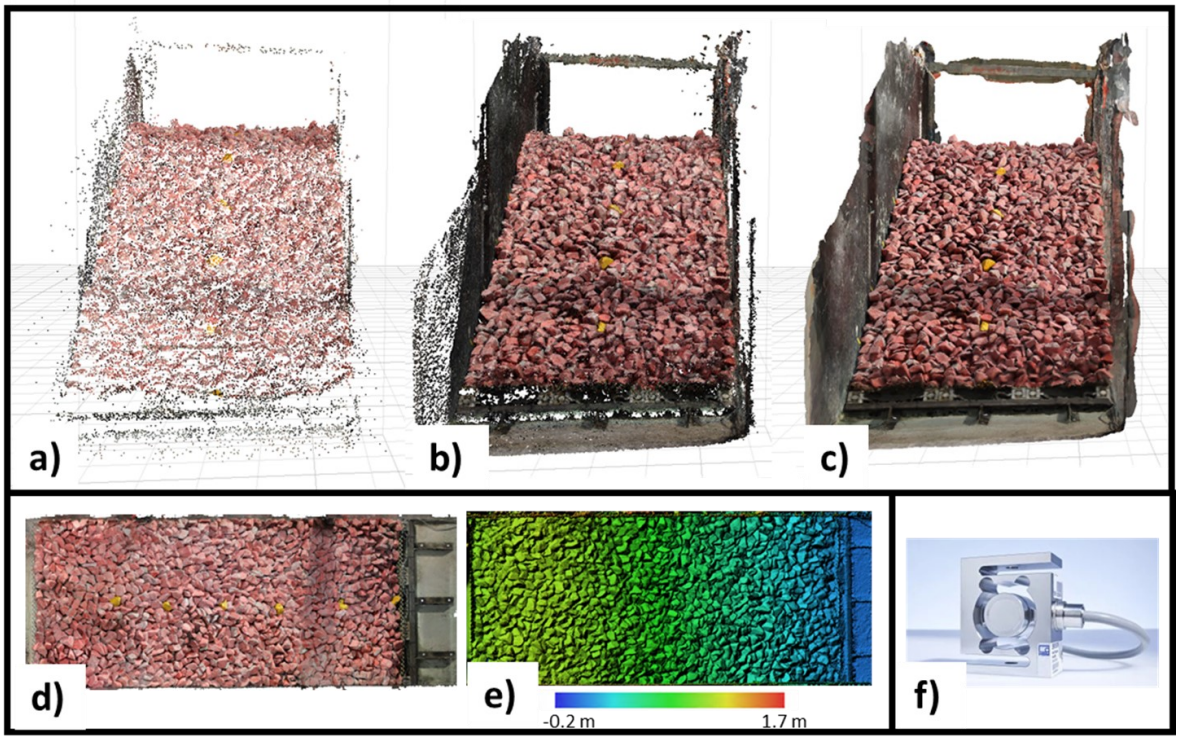

Figure 15. Main steps of Structure from Motion technique. Example for Test F before the first overtopping process (q_0). a) Tie points, b) dense cloud, c) 3D mesh, d) orthomosaic, e) digital elevation model and f) S9M force transducer. Dezert and Sigtryggsdóttir (2023).

In addition to the pictures taken between each discharge increase, 3 cameras were used to record the whole overtopping and breaching process and to provide complementary information on the failure mechanism. One was placed above the dam model and two were positioned outside the flume, recording through the glass wall of the left side of the flume. However, the images from those cameras were not used for 3D modelling. Complementarily, as it was done for M1-B models and in Ravindra et al. (2021), an automated 3D-traverse laser system was used to measure, between each discharge increase, the position of the 6 individual marked riprap stones placed in the center of the model (in yellow, Figure 15.c).

5.2 Data analysis

5.2.1 Axial reaction load at riprap toe

Once the models were built, the overtopping procedure could be carried out. After the opening of the pumps, the water level first overtops the core, generating throughflow inside the rockfill shoulder and then overtops the crest, provoking the overtopping phenomenon. Waterflow over the model induces an axial reaction load increase at the toe section. This axial reaction load is written F_i and expressed in Newtons. It was recorded for each of the four tests during the overtopping procedure and is displayed in Figure 16 according to discharge values. The critical loads, F_c, and critical discharges, q_c, correspond to values for which a complete failure occurs. These are displayed in Table 2 for the four tests. We observe an average critical discharge value of 200 $l.s^{-1}$ and critical load of 1 254 N for packed riprap layer (Tests F and G) and an average critical discharge value of 100 $l.s^{-1}$ and critical load of 1 150 N for non-packed riprap layer (Tests H and I).

Table 2. Critical discharges (q_c) and critical axial loads (F_c) for each of the four tests carried out on M4-C models. Dezert and Sigtryggsdóttir (2023).

Tests	Configuration	q_c ($l.s^{-1}$)	F_c (N)
T1	Placed packed	175	1218
T2	Placed packed	225	1290
T3	Placed non-packed	125	1290
T4	Placed non-packed	75	1010

Figure 16.a spotlights the strong linear relation between absolute axial loads and absolute discharge values for packed riprap layer (Tests F and G) with Nash–Sutcliffe coefficients $R^2 = 0.92$ and non-packed riprap layer (Tests H and I) with $R^2 = 0.95$. These results, put into perspective with the data from M1-B tests (Figure 16.a) display comparable trends but with greater absolute values. This increase can be imputed to the throughflow that was not occurring in previous studies where riprap and filter layer were built directly on the ramp without rockfill shoulder below. Figure 16.b displays the relative load values according to the relative water discharges. Expressed in a relative way, using critical discharges and critical load values, the difference between models with a rockfill shoulder and models without shoulder is not as important as it is with absolute values (Figure 16.a). Even a good

linear relation (Eq. 6, green trendline, Figure 16.b) can be proposed to describe the relation between these two parameters from the four tests (Tests F-I), with $R^2 = 0.87$:

$$\frac{F_i}{F_c} = 0.43\frac{q_i}{q_c} + 0.55 \quad (6)$$

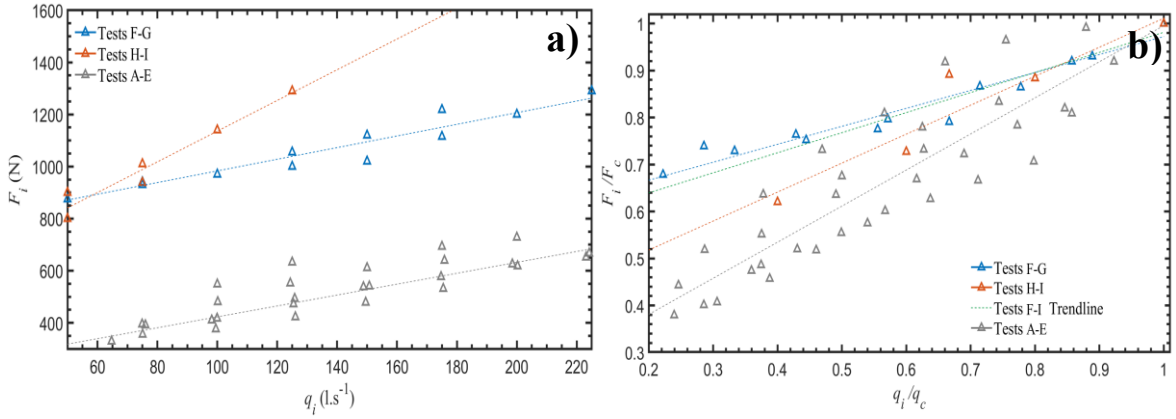

Figure 16. a) Absolute and b) relative axial loads at the toe section during overtopping phenomenon for the four tests. Comparison with the axial loads from M1-B model experiments for placed riprap models without rockfill shoulder (Tests A-E, in grey). Dezert and Sigtryggsdóttir (2023).

5.2.2 Buckling process and failure mechanism

Thanks to the 3D models of the rockfill dams built up in the laboratory (Figure 15.c), digital elevation models from each test (Figure 15.e) could be obtained. 3D models were carried out for initial structure, before overtopping, and in between each discharge increase. In Figure 17, we display for each test (Tests F-I) the difference of elevation between initial stage (q_0, before first overtopping process) and last stage (discharge value preceding critical discharge) with positive difference in white and negative difference in black. These correspond to the difference between $q_i = 150$ l.s^{-1} and q_0 for Test F, between $q_i = 200$ l.s^{-1} and q_0 for Test G, between $q_i = 100$ l.s^{-1} and q_0 for Test H and between $q_i = 50$ l.s^{-1} and q_0 for Test I. Also, every 10 cm along the x-axis, starting on the crest from x = 0 m, 4 positions of riprap stones (y = 0.2, 0.4, 0.6 and 0.8 m) were measured from these 3D models. From these coordinates, we were able to draw the orange vectors (Figure 17) standing for the displacement of these individual riprap stones along the slope from initial position before first overtopping to their last position before critical discharge value.

These figures highlight the non movement of riprap layer exposed to overtopping close to the toe support (right part of the figures) and on the crest (left part of the figures). However, the figures point out the progressive compaction of riprap along the slope, generating a gap close to the crest and inducing a buckling (as previously described in Ravindra et al. (2021)) towards the center of the model. It appears that the buckling is more important for Tests H and I than for Tests F and G even though the critical dischage values are lower for these tests. Also, the movement of individual stones along the y-axis is very limited for the four tests.

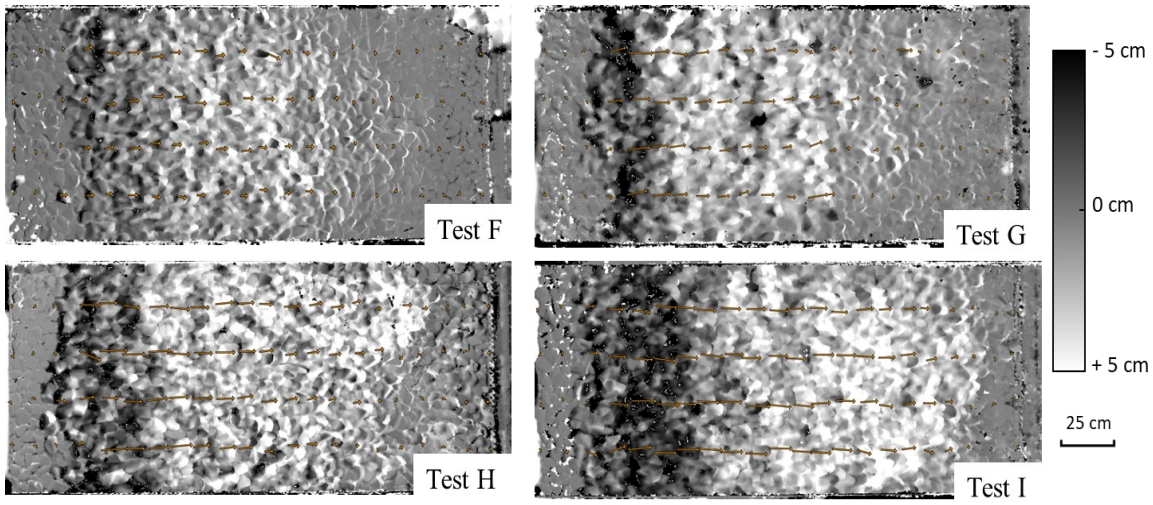

Figure 17. Highlighting of buckling process thanks to the differences of elevation for each test between initial position before overtopping (q_0) and last position before critical discharge (q_c) overtopping value (respectively corresponding to $q_i = 150$ l.s^{-1} for Test F, $q_i = 200$ l.s^{-1} for Test G, $q_i = 100$ l.s^{-1} for Test H and $q_i = 50$ l.s^{-1} for Test I). The orange vectors stand for the displacement of individual riprap stones on the x-y plane. Dezert and Sigtryggsdóttir (2023).

5.2.3 X and Z-displacements

From the obtained 3D models, plots displaying the displacement of the riprap layer in x and z-directions could be obtained (Figure 18), according to x positions (with x = 0 m standing for the upstream side of the crest). These are displacements between the initial position before overtopping and the ultimate position before critical discharge value (as the displacements displayed in Figure 17).

To obtain the Δz displacements (Figure 18.a-b), average z positions were extracted from the orthomosaics every 10 cm in the x-direction from x = 0 m to the toe support. The QGis

Profile tool was used to draw transverse profiles every 10 cm from one side of the flume to the other, to get an elevation profile and mean elevation values. This was done both for initial position (q_0) and for final position before the critical discharge overtopping event. The difference between final position and initial position elevations enables to obtain Δz values for each test (Figure 18.a) and average Δz values for all of them (Figure 18.b).

The Δx displacements (Figure 18.c-d) were obtained from the extracted x-coordinates from the orthomosaics of 4 individual riprap stones, selected every 10 cm in the x-direction at their initial position (q_0), for y = 0.2, 0.4, 0.6 and 0.8 m. In total, 88 stone positions were used on each model and their initial position correspond to the origin of the orange vectors displayed in Figure 17. The final x-positions of these stones were also extracted from the last orthomosaics before critical discharge overtopping event. The difference between the final and initial x-coordinates provides Δx values for each test (Figure 18.c) and average Δx for the four of them (Figure 18.d). In Figure 18.c, the Δx displacements of the 6 marked riprap stones (in yellow, Figure 15.c) from the laser measurement could also be plotted (represented as crosses) to be compared with data from the 3D models.

These plots highlight the good repeatability of these 4 tests concerning the x and z-displacements of the riprap layer. Indeed, the x-displacements of individual riprap stones could be described with an order 3 polynomial trendline (Figure 18.b), with $R^2 = 0.92$. Also, the z-displacement of the riprap layer can be described with an order 4 polynomial trendline, with $R^2 = 0.86$.

While all the tests do not seem to undergo important movement on the crest and close to the toe support, they all undergo a quite important compaction and buckling phenomenon that starts at the change of slope, after the crest (x = 0.3 m), generating a gap. Compaction in the x-direction tends to become less important as we get closer to the toe and the relative elevation of the layer appears to be more important in the middle of the downstream slope. We can observe that Tests 3 and 4 have their riprap layer more elevated over x = 1.20 m (Fig 18.a) and that the compaction along the slope is also more important for these tests than for Tests F and G (Fig 18.c).

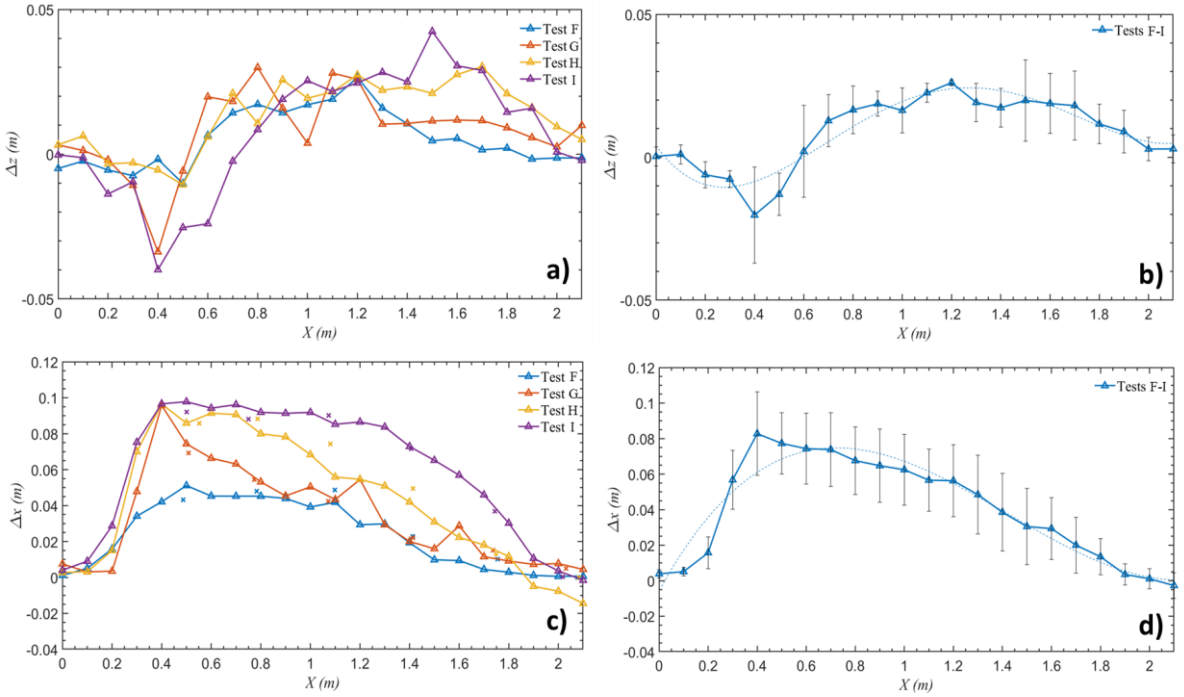

Figure 18. Z (a) and x displacements (c) of riprap for each individual test and average values for the four tests (b and d). c) The crosses stand for the displacement along the x-axis of individual riprap stones from laser measurements for tests F to I. The displacements were considered between initial position before overtopping (q_0) and last position before critical discharge (q_c) overtopping value (respectively corresponding to $q_i = 150$ l.s^{-1} for Test F, $q_i = 200$ l.s^{-1} for Test G, $q_i = 100$ l.s^{-1} for Test H and $q_i = 50$ l.s^{-1} for Test I). Dezert and Sigtryggsdóttir (2023).

6 Evaluation of the research findings and the NVE guidelines

Generally accepted principles to evaluate and model the flow through and over a riprap on steep slopes are not yet formulated. Due to high turbulence and a free water surface, Froude's model law can be used. To compare the different studies a stone related Froude number Fr_s, introduced in Eq. 7, is used. The critical discharge and the stone diameter are respectively q_c and d_s while the gravity acceleration is noted as g = 9.81 m.s^{-2}.

$$Fr_s = \frac{q_c}{\sqrt{g \cdot d_s^3}} \tag{7}$$

In these tests, the riprap stone diameter $d_s = d_{50}$ = 0.053 m is considered and the stone related Froude number for each test is displayed in Table 3.

Table 3. Critical discharge, critical load and stone related Froude number values for each experimental test from models M1-B (Tests A-E) and M4-C (Tests F-I).

	Test A	**Test B**	**Test C**	**Test D**	**Test E**	**Test F**	**Test G**	**Test H**	**Test I**
q_c **(l.s^{-1})**	225	325	200	350	150	175	225	125	75
Fr_s	5.89	8.5	5.23	9.16	3.93	4.58	5.89	3.27	1.96
F_c **(N)**	755	924	645	1040	812	1218	1290	1290	1010

For the four dam classes defined by the NVE (2012), specific recommendations are proposed for the sizing of riprap stones used as erosion protection on the downstream slopes of embankment dams in Norway. NVE defines the design situation with the minimum stone volume for consequence class 4, but design disharges for the other consequence classes. Placed ripraps need to be constructed on rockfill dam slopes with stones of volume of minimum 0.15 m^3 (D_{min} = 0.64 m) for dams classified within consequence class 4. To determine the stone size for dams in class 3 and 2, Eq. 8 can be used assuming a minimum unit discharge q of 0.5 m^3.s^{-1} for Class 3 and Class 2 and 0.3 m^3.s^{-1} for Class 1 (Table 4).

$$D_{min} = S^{0.43} \cdot q^{0.78} \quad (8)$$

With the slope value S = 0.67 in the tests and D_{min} the riprap size for full scale dams. D_{min} values for each dam class and associated discharge scaling factor, S_f, are displayed in Table 4 such as:

$$S_f = \sqrt{\left(\frac{D_{min}}{d_{50}}\right)^3} \quad (9)$$

Table 4. Computed minimum riprap size values for each consequence class dam.

	Class 1	**Class 2**	**Class 3**	**Class 4**
Design discharge ($m^3.s^{-1}.m^{-1}$)	0.3	0.5	0.5	0.7
***D_{min}* (m) (NVE)**	0.33	0.49	0.49	0.64
S_f	15.53	28.11	28.11	41.96

From Eq. 7, with these D_{min} (Table 4) values and stone related Froude numbers (Table 3), the critical discharge values scaled for each consequence class dam from the 9 experimental tests can be computed and are displayed in Table 5 (A-E) and 6 (F-I).

Table 5. Critical discharge values ($m^3.s^{-1}$) per meter, from each individual test from model M1-B, corresponding to the four consequence class dams using Froude scaling law, with associated mean and standard deviation values.

	Test A (q_c)	**Test B (q_c)**	**Test C (q_c)**	**Test D (q_c)**	**Test E (q_c)**	$\overline{q_c}$	σ_{q_c}
Class 1	3.48	5.03	3.09	5.41	2.32	**3.87**	1.17
Class 2	6.33	9.14	5.62	9.84	4.22	**7.03**	2.13
Class 3	6.33	9.14	5.62	9.84	4.22	**7.03**	2.13
Class 4	9.44	13.64	8.39	14.69	6.29	**10.49**	3.18

Table 6. Critical discharge values ($m^3.s^{-1}$) per meter, from each individual test from model M4-C corresponding to the four consequence class dams using Froude scaling law, with associated mean and standard deviation values.

	Test F (q_c)	**Test G (q_c)**	**Test H (q_c)**	**Test I (q_c)**	$\overline{q_c}$	σ_{q_c}
Class 1	2.71	3.48	1.93	1.16	**2.32**	0.86
Class 2	4.92	6.33	3.51	2.11	**4.22**	1.57
Class 3	4.92	6.33	3.51	2.11	**4.22**	1.57
Class 4	7.34	9.44	5.25	3.15	**6.29**	2.35

As a comparison, from the previous study with placed riprap unsupported at the toe (Ravindra et al., 2020), the associated critical discharge values obtained were 0.84 $m^3.s^{-1}$ for consequence class 1, 1.51 $m^3.s^{-1}$ for consequence class 2 and 3, 2.26 $m^3.s^{-1}$ for consequence class 4. Also, for placed riprap with dam unsupported at the toe, the associated critical discharge values were 0.42 $m^3.s^{-1}$ for consequence class 1, 0.76 $m^3.s^{-1}$ for consequence class 2 and 3, 1.13 $m^3.s^{-1}$ for consequence class 4 (Ravindra and Sigtryggsdottir, 2021).

Safety Factors (Table 7) can be computed as ratios of the scaled discharge levels (Tables 5 and 6) and the NVE recommended design discharge magnitudes (Table 4). The safety factors enhance to evaluate the critical discharges against the recommendations proposed by the NVE (Table 4). The scaled discharges for all 4 dam consequence classes (Table 7) from the 5 tests (A-E) with M1-B models were found to exceed the NVE recommended design discharge values and display a resistance almost five time superior to the resistance of unsupported placed riprap (M2). Similarly, the scaled discharges from the 4 tests (F-I) with M4-C models exceed the NVE recommended design discharge values with a resistance at least six times superior to the resistance of dam with unsupported placed riprap (M4-A).

Table 7. Details of safety factors computations for 4 consequence classes for placed riprap with and without toe support.

	Class 1	Class 2	Class 3	Class 4
Placed riprap with fixed toe support (M1-B)	12.89	14.06	14.06	14.99
Placed riprap unsupported at the toe (Ravindra et al., 2020) (M2)	2.8	3	3	3.2
Placed riprap with dam supported at the toe (M4-C)	7.73	8.43	8.43	8.99
Placed riprap with dam unsupported at the toe (Ravindra and Sigtryggsdottir, 2021) (M4-A)	1.4	1.5	1.5	1.6

From the critical axial load values acquired on the model and displayed in Table 3, it is also possible to estimate the critical load values that would correspond to full scale dams of different classes from the experimental tests. Considering the scaling law expressed in Eq. 10, the critical axial load values (in kN) are displayed in Tables 8 and 9.

$$F_{c,prototype} = F_{c,model}\left(\frac{D_{min}}{d_{50}}\right)^3 \quad (10)$$

Considering that the model built in the flume is a 1:10 scale model of a dam, it is also possible to compute the q_i (l.s^{-1}) and F_i (N) values from the scaling laws introduced above, Eq. 10. Such values for a full-scale dam ten times bigger than the experimental model (considering $d_{50,fullscale\ dam}$= 0.53 m) are displayed Figure 19. Total axial load values would have to be divided by 10 to get the critical scaled load values (in kN/m) for a 1 m width section of a 10 meters width dam.

Table 8. Critical total axial load values from each individual test for model M1-B (A-E) corresponding to the 4 consequence class dams after scaling, with associated mean and standard deviation values for the whole dam (kN) as well as average critical load value for a 1 m width section (kN/m).

	Test A (F_c)	**Test B** (F_c)	**Test C** (F_c)	**Test D** (F_c)	**Test E** (F_c)	$\overline{F_c}$ [kN]	σ_{F_c} [kN]	$\overline{F_c}$ [kN/m]
Class 1	181	221	154	249	194	200	33	**32**
Class 2	598	731	510	823	643	661	108	**71**
Class 3	598	731	510	823	643	661	108	**71**
Class 4	1 329	1 627	1 136	1 831	1 430	1 471	240	**122**

Table 9. Critical total axial load values from each individual test for model M4-C (F-I) corresponding to the 4 consequence class dams after scaling, with associated mean and standard deviation values for the whole dam (kN) as well as average critical load value for a 1 m width section (kN/m).

	Test F (F_c)	**Test G** (F_c)	**Test H** (F_c)	**Test I** (F_c)	$\overline{F_c}$ [kN]	σ_{F_c} [kN]	$\overline{F_c}$ [kN/m]
Class 1	292	309	309	242	288	27	**46**
Class 2	964	1021	1021	799	951	90	**103**
Class 3	964	1021	1021	799	951	90	**103**
Class 4	2145	2271	2271	1778	2116	202	**175**

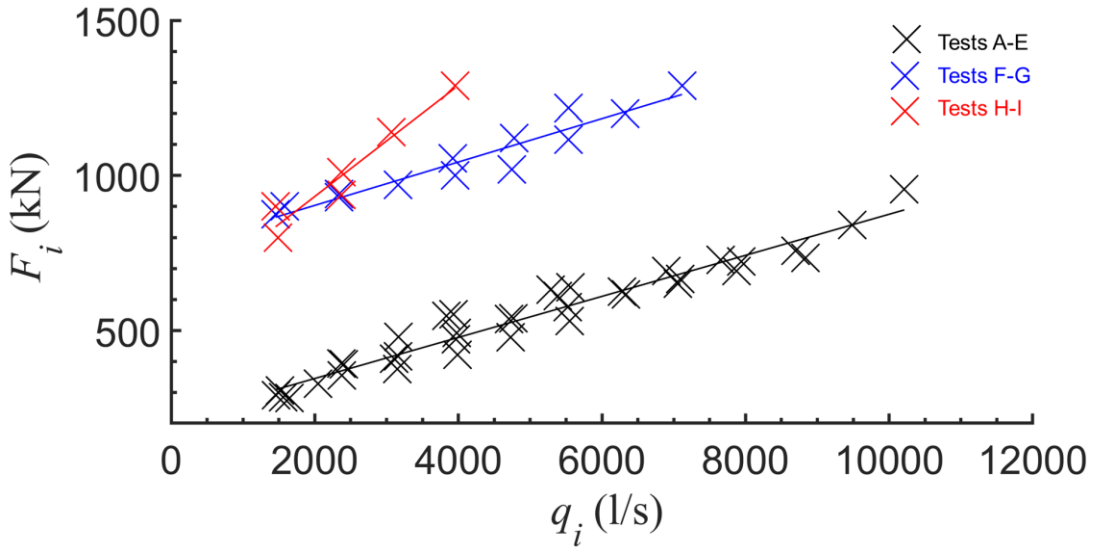

Figure 19. Scaling of the total axial load at the toe section during overtopping event according to discharge values. Data extracted scaled for a dam ten times bigger (i.e., 10 m width) than the experimental model considered in this work.

In addition to the design situation with the design discharges in Table 4, the NVE (2012) defines safety check discharges for accidental leakages and/or overtopping. The safety check disharges are 10 m^3/s for consequence class 4 and 3, 5 m^3/s for consequence class 2 and 1 m^3/s for consequence class 1. The safety check discharges are generally transferred to unit discharges considering the length of relevant zone of the dam experiencing the accidental leakage/overtopping. The resulting unit discharge values of the accidental leakage/overtopping can be inserted into Eq.(8) to calculate the riprap stone sizes required for the safety check. .

7 Discussion

7.1 Summary of critical discharges and loads across model setups

It is possible to put into perspectives the critical discharge values from M1-B and M4-C models compared to the other models previously built up (Table 10). Indeed, it is interesting to point out that for all models, considering same toe support condition and same riprap type, the average critical discharge value is two times less important when the riprap layer is built on a rockfill dam model.

Also, it should be highlighted that from these new tests we can observe a relation between critical discharges from unsupported riprap test and critical discharges from supported ones. Thus, the average discharges withstood by the supported models with placed riprap are five times greater than the unsupported ones (60 $l.s^{-1}$ for unsupported placed riprap and 275 $l.s^{-1}$ for supported placed riprap, 30 $l.s^{-1}$ for unsupported placed riprap with dam and 150 $l.s^{-1}$ for supported placed riprap with dam). These results directly demonstrate the importance of the presence of toe support to enhance the stability of rockfill dams with erosion protection comprising placed riprap.

Concerning the critical load (Table 3), the values should be considered differently than the critical discharges for M1-B and M4-C models. Even though the critical discharges are lower for F-I tests (150 $l.s^{-1}$) compared to A-E tests (250 $l.s^{-1}$), such difference is not observed for critical load values (835.2 N for A-E tests and 1202 N for F-I tests). In fact, the load values are higher for M4-C models because of the throughflow that is absent from A-E tests with M1-B models. The importance of pore pressure on slope stability was already demonstrated by Worman (1993) and Morán and Toledo (2011). This work is also along these lines. The introduction of a high permeability toe drain within the dam could be helpful to reduce the pore pressure and improve the dam stability, as suggested by Kiplesund et al. (2021).

Table 10. Summary of critical discharges values and failure mechanism for different model setup.

Toe support condition	Riprap type	Model setup	Average q_c ($l.s^{-1}$)	Failure mechanism
Unsupported	Dumped on ramp	M2	40	Surface erosion
Unsupported	Dumped with dam shoulder	M4-A	17.5	Surface erosion
Unsupported	Placed on ramp	M2	60	Sliding
Unsupported	Placed with dam shoulder	M4-A	30	Sliding
Supported	Placed on ramp	M1-A and M1-B	275	Buckling
Supported	Placed with dam shoulder	M4-C	150	Buckling

7.2 Role of the riprap packing

(The discussion in this section on M4-C is adapted from Dezert and Sigtryggsdóttir (2023)).

Regarding previous research works carried out within the NTNU hydraulic laboratory, it is the first time that two different building processes were used for placing riprap stones. While Tests F and G had their riprap layer packed during construction, Tests H and I did not. From the obtained results, it appears that packing has an important impact on the stability of the structure even though the failure mechanism is the same for the four tests. Indeed, the critical discharge values range from q_c = 175 to 225 $l.s^{-1}$ for packed riprap layer (Tests F-G) while they range from q_c = 75 to 125 $l.s^{-1}$ for non-packed riprap layer (Tests H-I). However, the critical load values (Table 2) do not appear to be impacted the same way by the building procedure. Indeed, the critical load values range from F_c = 1 218 to 1 290 N for packed riprap layer (Tests F-G) and from F_c = 1 010 to 1 290 N for non-packed riprap layer (Tests H-I). Thus, even though the absolute measured axial load values (Figure 16.a) tend to increase

faster for non-packed models as the overtopping discharge increases, the critical load (F_c) measured are quite comparable for both types of construction.

This outcome is in accordance with the results from M1-B models where it is highlighted that most of the axial load measured at the toe comes from the compaction of the riprap layer and not directly from the hydraulic load of the overtopping water (Figure 8). Indeed, limited discharge flow on non-packed riprap layer can induce the same load measured at the toe as the one that could be measured for higher overtopping discharge on packed riprap layer. This is directly related to the importance of the compaction/buckling phenomenon observed on the models. As displayed in Figures 17 and 18.c, the non-packed models (Tests H-I) undergo a compaction phenomenon faster and of greater amplitude than the packed ones (Tests F-G), for lower discharge levels. The results from Figure 18 suggest that Test I was the less packed model since it underwent i) the most important compaction in the x-direction (Figure 18.c), ii) the most important generated gap at the top of the downstream slope at x = 0.4 m (Figure 18.a) and iii) the most important buckling evidence with an elevation at x = 1.5 m (Figure 18.a). It is then interesting to observe that this model was the first one to break, with q_c = 75 $l.s^{-1}$. Also, it can be observed that the riprap layer of packed models appears to elevate more in the first half of the downstream slope while almost the whole layer is concerned with the elevation of riprap stones for non-packed models (Figure 17).

The trendlines displayed in Figure 18 enable to display the maximum x and z-displacements tolerated by the dam models before failure. The relation is in pretty good adequation for both packed and non-packed dams. This highlights the fact that studying the movement of the riprap layer could be more valuable to estimate the moment of rupture than a theoretical maximum critical discharge value that could vary a lot according to the building process.

7.3 Axial reaction loads at riprap toe

(The discussion in this section on M1-B is adapted from Dezert et al. (2022) and Dezert and Sigtryggsdóttir (2023)).

First, from all the axial load values measured at the toe section in this study for M1-B model, it is important to point out that a stabilization of these values is observed (Figure 5) quite soon during the building of the riprap layer (around 50 cm from the toe). Such behavior could be explained by the compensation of the self-weight of the riprap stones by both the

friction with the filter layer and the interlocking pattern of the placed riprap. Indeed, Hiller et al. (2018) depicted that the interlocking of the riprap stones induces the transfer of longitudinal forces within the whole layer. Once a threshold value of building length is reached for the riprap layer, adding more stones has no significative impact on the measured axial load at the toe. Such value is a function of the considered interlocking pattern and can vary according to the configuration of the stones at the toe. For example, Khor (2008) specifically displays the variability of the mechanical and structural properties of different interlocking patterns. Also, from studies on experimental model without toe support (Ravindra et al., 2020), the specificity of the pattern of placed riprap explains why it can resist up to 1.5 times greater discharge values than dumped riprap.

Further, the results display a very strong linear relation between critical water discharge and critical axial load values measured at the toe. This relation can be observed for each individual test (Figure 7.a-e) but also for the global dataset (Figure 7.f) for model M1-B. It is important to highlight the fact that even though the building and testing procedures were supposed to be similar, the five experimental models underwent a breakage for different critical discharge and axial load values (Table 3). The variability of values can be imputed to the variability in the construction stage where axial load values are already slightly different from one test to another (Figure 5). Still, the relation described in Eq. 2 between the two physical parameters appears pertinent when used for the buckling deformation analogy (Eq. 5). However, this relation must be put into perspective with the multiple contributions of axial load. Figure 8 points out that even though the discharge level plays an important role in the total axial load measured at the toe, the load increase imputed to the deformation of the riprap layer, FR_i, is greater than the contribution from the waterflow, FW_i. Indeed, between each discharge step when the waterflow is stopped, the measured axial load does not come back to its initial value (Figure 6.a). This means that both the compression (Figure 9) and the elevation (Figure 10) of the riprap stones induce an additional load. Since Tests A-E were non-packed, they should be compared with Tests H and I built on a rockfill shoulder. While the mean critical load value for models built on a rockfill shoulder is $\overline{F_c}$ = 1 254 N (Tests H-I), models built on a ramp are associated with lower axial load values, with $\overline{F_c}$ = 835 N (Tests A-E). This difference can be imputed to the presence of throughflow in this research work. Such phenomenon was not occurring in the experiments carried out with M1-B models and the absolute load data comparison is striking in Figure 16.a. These results

point out how important it is to study the behavior of riprap structure on a rockfill shoulder to be able to take the effect of throughflow into consideration. Still, it can be observed that when comparing the absolute load values (Figure 16.a), the trends are the same for packed placed riprap (Tests F-G, in blue) and for non-packed placed riprap on a ramp (Tests A-E, in grey); while the axial load increase appears to be faster for non-packed riprap with a shoulder (Tests H-I, in orange). This is directly related to the important compaction that occurs at low discharge for the non-packed tests (Figure 17), significantly increasing the load values because of the riprap compaction. However, we should highlight that the load data from non-packed tests (Tests H-I) fit well in the data from M1-B tests when considered as relative values (Figure 16.b), because of a quite low critical discharge value associated with.

7.4 Deformation behavior related to buckling process

(The discussion in this section on M1-B is adapted from Dezert et al.(2022)).

As Ravindra et al. (2021) demonstrated the relation between overtopping discharge level and deformation of the riprap layer, the results displayed for M1-B model demonstrate a very strong relation between axial load at the toe section and deformation of the placed riprap. The deformation of the riprap layer can be observed in 2D thanks to the measurement of specific riprap stone positions. It appears that the rocks undergo a compression along the *x*-axis (Figure 9) that can be imputed to both the gravity as well as to the hydraulic drag and lift forces during the successive overtopping events. The stones also undergo a progressive elevation (Figures 10 and 11) because of the hydraulic lift forces that tend to elevate the stones along the *z*-axis. However, the interlocking forces tend to counter that effect vertically and generate a bearing structure that can resist important loads thanks to the possible deformation of the whole riprap layer. The compression in the *x*-direction of the layer can be related to the axial load values (Eq. 3), as it was previously done by Ravindra et al. (2021) for discharge values. The exponential increase of the horizontal compaction according to axial load values is common to all tests but quite important differences can be observed between each test. Furthermore, the dispersion of the dataset around the exponential regression curve (Figure 9.f) implies to carefully consider the relation (Eq. 3) between these

two parameters. Still, the relation between discharge value and displacement in *x*-direction established by Ravindra et al. (2021), once adapted from Eq. 2, is quite close to the results.

Ravindra et al. (2021) first pointed out a buckling analogy for 2D deformation of placed riprap supported at the toe when exposed to overtopping. Considering a similar experimental procedure, a buckling process can also be observed from the results displayed in Figures 10 and 11. The buckling analogy consists in comparing the riprap layer to a slender-long column, free at one end and maintained at the other. Here, the free end would correspond to the top part of the riprap layer while the pinned end would be the stones lying on the metallic support at the toe. The riprap stones located in the center of the riprap layer globally undergo a relative elevation greater than the one undergone by the stones at both ends of the layer (Figures 10 and 11). In this work, the buckling process can also be observed when the displacement values are put in perspective with axial load values and not only discharge values. When organized together, regarding load intervals from each of the five tests, the displacement of riprap stones can be characterized using Eq. 5 (Figure 12). This relation was made possible from the relation defined by Ravindra et al. (2021) and by the relation between axial load and discharge values from Eq. 2. The fitting of the data is not optimal for smaller loads (Figure 12) as it was observed in Ravindra et al. (2021). This can be explained by the gaps present in the structure because of some loosely placed stones. The initial displacements of the riprap stones during the initial overtopping is then more complicated to predict. It achieves a stable buckling profile at higher discharges.

These displacement data and this buckling observation make this study consistent with previous research works but also enables the understanding of the load contribution, FR_i, from Figure 8. Indeed, the relative elevation of the riprap stones from the center of the structure compared to the riprap stones from the toe (Figure 11) corresponds to an increase of the slope of the riprap column. Also, the elevation of riprap stones induces less friction with the filter layer. These two processes together result in that a larger of the riprap weight (component parallel to the slope) is carried by the support as well as compaction of the riprap against the toe support, and thus induce an increase of the axial load in the *x*-direction, perpendicular to the metallic toe support, where the load cells are located.

However, no strong relation between axial load at the toe and individual riprap displacement could be observed when the riprap layer is built on a rockfill shoulder. The validity of the

buckling equation (Eq.5) for models built on a ramp does not apply in such half-dam models even though an axial load increase can also be observed and directly related to the buckling deformation of the riprap layer on such models.

7.5 Use of Structure from Motion technique

(The discussion in this section on M4-C is adapted from Dezert and Sigtryggsdóttir (2023)).

The Structure from Motion technique has proven itself to be very effective for the purpose of studying riprap displacement under overtopping conditions. Much more coordinates could be collected from the generated 3D models for Tests F-I than what was done with the laser for Tests A-E. Also, we could demonstrate that the laser measurements are consistent with the extracted coordinates from the orthomosaics (Figure 18.c). This technique is more reliable for statistical and global analysis of the riprap layer. It is indeed more valuable to look at many individual stones instead of few of them that may not be representative of the whole protective structure's behavior. The use of DEMs difference is also very explicit (Figure 17) to observe the buckling phenomenon.

Furthermore, in the future, it would eventually be possible to reuse the generated 3D models to investigate other topics of interest or for new comparisons with other models. The Structure from Motion technique could also provide information on a potential dam rupture if large movements of riprap are observed between two 3D models compared at different time steps.

7.6 Recommendations and limitations

First, it must be insisted that the validity of this research outcome is limited to dam models with the specific material physical parameters, dimensions and slope values indicated in the experimental set up and methodology sections. Different parameters could bring different results, especially if the riprap stones have a different shape and are rounded. Then they can not interlock as they do in our methodology.

Both the placed riprap supported at the toe without dam from model M1-B and with dam from model M4-C, withstand the design discharge values given by the NVE (2012) regulations for sizing of riprap (Table 4) with Eq.8. Model M1-B withstands with a high

safety factor of 14.0 on the average (Table 7), while unsupported riprap has a factor of safety of 3.0 on the average (Table 7). On the other hand, Model M4-C display safety factor values of 8.40 on the average, while unsupported riprap with dam has a safety factor of 1.5.

The scaling of axial load values (Table 8, 9 and Figure 19) enables to understand the axial load that the respective consequence classes dams could withstand before breakage if supported at the toe. However, it is worth noting that from a field survey carried out by Ravindra et al. (2019), most Norwegian dams are not supported at the toe. Such information may be useful to establish new recommendations for the future.

For M1-B model, thanks to the five experimental tests carried out, the good repeatability of the results can be discussed. The range of critical discharge values goes from 150 to 350 $l.s^{-1}$, which is quite comparable to the range of critical discharge values Ravindra et al. (2021) display in their previous study (120 to 300 $l.s^{-1}$). The range of critical axial load values goes from 645 to 1 040 N. The variability of F_i values (Figures 5 and 7) between each test shows that even though the building procedure is the same, the perfect repeatability of each experiment cannot be granted. The construction of the model cannot be repeated the same way according to the experience of the builder and to the exact arrangement of the materials. Thus, the position of individual placed riprap stone is different from one model to another. Even though the riprap shoulder is built so as riprap stones are interlocked as well as possible, it is more likely that if some stones are locally badly interlocked together in a model, they can collapse at middle discharge levels. Then, a part of the dam is left unprotected, generating the sliding of the riprap stones above and the complete failure of the work. Nonetheless, it is important to indicate than no relation can be established between the packing factor values (Table 1) and the critical discharge values. Also, even though each model is slightly different, the relation described between the studied physical parameter display the same trends (Figures 5, 7, 8, 9 and 12).

8 Concluding summary

The objective of this and previous related research projects at NTNU is to provide more information on rockfill dams exposed to overtopping events. Several experimental models (M1, M2, M3 and M4) as well as field surveys were carried out within these projects. One of the interests of such experiments is to be able to predict the resistance of rockfill dam against overtopping according to different setups. In this report, we particularly took an interest in understanding placed riprap failure mechanisms with the introduction of placed riprap supported at the toe and built on a ramp (M1-B) and placed riprap supported at the toe with the presence of a rockfill shoulder (M4-C). All the models were exposed to successive and increasing overtopping water discharge until complete failure of the structure, while measuring the axial load at the toe section and the displacement of individual riprap stones.

Five M1-B models and four M4-C models were built in the hydraulic laboratory of the Norwegian University of Science and Technology. The results and the interpretation from M1-B tests demonstrated a strong relation in each test between axial loads measured at the toe, individual riprap stone displacements and water discharge level. When discriminating the contribution of load from the water and from the riprap stones, it also appeared that the contribution of the load induced by the deformation of the riprap layer is greater than the contribution from the hydraulic load. Furthermore, the deformation qualified as a buckling by Ravindra et al. (2021) has also been observed as it was from M1-A tests. The buckling tends to increase the axial load measured at the toe after every overtopping stage. Moreover, the interlocking pattern of the placed riprap stones acts as a bearing structure and induced a stabilization of the axial load measured at the toe during the building stage. The results from M4-C tests demonstrate a strong linear relation between axial loads measured at the toe and overtopping discharges for both packed and non-packed riprap layers. The importance of throughflow mechanisms in the rockfill shoulder was brough to light by comparing these results with data from M1-B models. It appears that such throughflow mechanism tends to increase the absolute axial loads at the toe.

The Structure from Motion technique could highlight the sliding and buckling process of the riprap layer that had not been previously observed for riprap built on a rockfill shoulder. The use of this technique is innovative to follow the displacement of riprap stones and proved to

be much more efficient than the use of laser system to point individual rocks. It was demonstrated that the sliding mechanism is more important (both in z and x-directions) and appears at lower overtopping discharges for non-packed placed riprap layer. However, no clear relation could be demonstrated between riprap stone displacement (buckling process) and axial load values from M4-C models. Still, for the four models (both packed and non-packed riprap layers), similar trends for x and z-displacements of the riprap were demonstrated between initial position and last position before failure. Such information suggest that the critical discharge value is not as reliable as the riprap displacement to predict the dam failure.

Critical discharge and load values were also put into perspective with NVE recommendations for full scale dams from both M1-B and M4-C models. They suggest that all consequence class dams would resist the design overtopping discharge level (Table 4) requested for dimensioning of placed riprap stones on the downstream slope of embankment dams in Norway. However, it will depend on individual dam site whether NVE's safety check discharge values for accidental overtopping and leakage are resisted.

The obtained results and associated scientific discussion, when corroborated by additional data on complementary tests, could be valuable to improve the understanding of riprap stability on rockfill dams as well as to provide suggestions for dam design and reinforcement techniques. Still, the reader must keep in mind that the results from this report apply only to experiments conducted on experimental dams built with specific material and slope characteristics. The use of such results and interpretations for a real dam case study should be considered with caution.

Acknowledgement

We would like to thank Mahlet Kinfe Gebreegziabher, Mahta Samie and Jan Hřebřina for their precious help during the building of M4-C models. We acknowledge the contribution from Ganesh H.R. Ravindra and Priska Hiller, as well as the authors of the MSc thesis listed in this report to the related research projects at NTNU. The authors gratefully thank the master student Kofi Ntow Opare for assistance in carrying out the M1-B experiments together with and under the supervision of Ganesh H.R. Ravindra.

The experimental work presented was carried out as a part of Work Package 1, Project 1.2 Dam construction and Dam safety within HydroCen, Norway. The writing of this report is made possible with the financial support offered by the Norwegian Water Resources and Energy Directorate (NVE), Hafslund E-CO Vannkraft, Hydro Energi, NEAS, SFE Produksjon, Sira-Kvina, Skagerak Kraft AS, Statkraft, Tafjord Kraftproduksjon, and Trønder Energi, all in Norway.

References

Abt, S. R., & Johnson, T. L. (1991). Riprap design for overtopping flow. *Journal of hydraulic engineering*, *117*(8), 959-972.

Abt, S. R., Thornton, C. I., Scholl, B. A., & Bender, T. R. (2013). Evaluation of overtopping riprap design relationships. *JAWRA Journal of the American Water Resources Association*, *49*(4), 923-937.

Abt, S.R.; Thornton, C.I. Riprap Design for Overtopping—Man Do I Need a Martini! (2014). *World Environ. Water Resour. Congr.* 191–1198.

Agisoft LLC Agisoft Metashape User Manual Professional Edition, Version 1.7. Agisoft Metashape (2021), 160.

Bunte, K.; Abt, S.R. Sampling Surface and Subsurface Particle-Size Distributions in Wadable Gravel and Cobble-Bed Streams for Analyses in Sediment Transport, Hydraulics, and Streambed Monitoring (2001). US Department of Agriculture, Forest Service, Rocky Mountain Research Station, Fort Collins, Colorado, United States, 2001.

Dezert, T.; Ravindra, G.H.R., Sigtryggsdóttir, F.G. Placed Riprap Deformation Related to Axial Load at Toe Support: Physical Modelling (2022). *Water*, 14, 1581.

Dezert, T.; Sigtryggsdóttir, F.G. 3D displacement and axial load of placed riprap supported at the toe: use of structure from motion (2023). *Journal of Hydraulic Engineering, 150(1)*.

Dornack, S. Uberstrombare Damme-Beitrag zur Bemessung von Deckwerken aus Bruchsteinen/ Overtopping Dams-Design Criteria for Riprap. (2001). Ph.D. Thesis, Technische Universitat Dresden, Germany.

Hiller, Priska H. (2017). Riprap design on the downstream slopes of rockfill dams,. *Doctoral Thesis, Norwegian University of Science and Technology, Trondheim*.

Hiller, Priska H, Aberle, J., & Lia, L. (2018). Displacements as failure origin of placed riprap on steep slopes. *Journal of Hydraulic Research*, *56*(2), 141–155.

Hiller, P. H., Lia, L., & Aberle, J. (2019). Field and model tests of riprap on steep slopes exposed to overtopping. *Journal of Applied Water Engineering and Research*, 7(2), 103-117.

ICOLD. Dam Failures—Statistical Analysis; Bulletin 188; ICOLD: Paris, France, (2021).

Jandora, J.; Říha, J. The Failure of Embankment Dams Due to Overtopping. (2008). Vutium: Brno, Czec Republic.

Khan, D., & Ahmad, Z. (2011). Stabilization of angular-shaped riprap under overtopping flows. *World Academy of Science, Engineering and Technology*, *59*, 1153-1157.

Khor, H.C. Mechanical and Structural Properties of Interlocking Assemblies. (2008). Ph.D. Dissertation, University of Western Australia, Perth, Australia.

Kiplesund, G. H., Ravindra, G. H., Rokstad, M. M., & Sigtryggsdóttir, F. G. (2021). Effects of toe configuration on throughflow properties of rockfill dams. *Journal of Applied Water Engineering and Research*, *9*(4), 277-292.

Kiplesund G.H., Sigtryggsdóttir F.G. and Lia L. (2022). Breach progression observation in rockfill dam models using photogrammetry. Submitted manuscript in Remote Sensing. MDPI journal.

Knauss, J. Computation of maximum discharge at overflow rockfill dams (a comparison of different model test results). (1979). In *13th Congress on Large Dams*; International Comission on Large Dams, New Delhi, India, Volume Q50, pp. 143–159.

Kobayashi, N., & Jacobs, B. K. (1985). Riprap stability under wave action. *Journal of waterway, port, coastal, and ocean engineering*, *111*(3), 552-566.

Larsen, P.; Bernhart, H.H.; Schenk, E.; Blinde, A.; Brauns, J.; Degen, F.P. (1986). Uberstrombare Damme, Hochwasserentlastung Uber Dammscharten/Overtoppable Dams, Spillways over Dam Notches. Prepared for Regierungsprasidium Karlsruhe, Universita. Unpublished Report.

Lia, L., Vartdal, E. A., Skoglund, M., & Campos, H. E. (2013). Riprap protection of downstream slopes of rockfill dams-a measure to increase safety in an unpredictable

future climate. *European Club Symposium of the International Comission on Large Dams*.

Morán R, Toledo MÁ. (2011). Research into protection of rockfill dams from overtopping using rockfill downstream toes. Can J Civ Eng. 38(12):1314–1326. DOI:10.1139/L11-091.

Najafzadeh, M.; Oliveto, G. (2020). Riprap incipient motion for overtopping flows with machine learning models. *J. Hydroinformatics*, *22*, 749–767.

NVE. (2012). Veileder for fyllingsdammer. *Norwegian Water Resources and Energy Directorate*, 21–25.

Olivier, H. (1967) Through and Overflow Rockfill Dams-New Design Techniques. *Proc. Inst. Civ. Eng. 36*, 433–471.

Peirson, W.L.; Jens, F.; Steven, E.P.; Ronald, J.C. (2008). Placed Rock as Protection against Erosion by Flow down Steep Slopes. *J. Hydraul. Eng. 134*, 1370–1375.

Ravindra, G. H., Sigtryggsdottir, F. G., Asbølmo, M. F., & Lia, L. (2019). Toe support conditions for placed ripraps on rockfill dams-A field survey. *Vann*, *3*, 185-199.

Ravindra, G.H.R.. Hydraulic and Structural Evaluation of Rockfill Dam Behavior When Exposed to Throughflow and Overtopping Scenarios. (2020). Ph.D. Thesis, Norwegian University of Science and Technology, Trondheim.

Ravindra, G. H. R., Gronz, O., Dost, B., & Sigtryggsdottir, F. G. (2020). Failure mechanism in placed riprap on steep slope with unsupported toe. *Engineering Structures*

Ravindra, G.H.R.; Sigtryggsdottir, F.G.; Lia, L. (2021). Buckling analogy for 2D deformation of placed ripraps exposed to overtopping. *J. Hydraul. Res. 59*, 109–119.

Ravindra, G. H. R., & Sigtryggsdottir, F.G. (2021). Rockfill dams – downstream riprap and dam toe : FoU-project 80409. NVE Ekstern rapport nr. 17/2021.

Siebel, R. (2007). Experimental investigations on the stability of riprap layers on overtoppable earthdams. *Environmental fluid mechanics*, *7*(6), 455-467.

Sommer, P. (1997). Uberstrombare Deckwerke/Overtoppable Erosion Protections. No. DFG-Forschungsbericht La 529/8-1, Universita. Unpublished Report.

Stephenson, D.J. (1979). *Rockfill in Hydraulic Engineering*; Elsevier: Amsterdam, The Netherlands.

Thielicke, W. (2014). The flapping flight of birds Summary and Conclusions. *PhD Thesis, Rijksuniversiteit Groningen*.

Thornton, C. I., Abt, S. R., Scholl, B. N., & Bender, T. R. (2014). Enhanced stone sizing for overtopping flow. *Journal of hydraulic engineering*, *140*(4), 06014005.

Worman A. (1993). Seepage induced mass wasting on coarse soil slopes. Journal of Hydraulic Engineering. 119(10):1155– 1168.

NVE

Norges vassdrags- og energidirektorat

Middelthuns gate 29
Postboks 5091 Majorstuen
0301 Oslo
Telefon: (+47) 22 95 95 95